NAVAL POSTGRADUATE SCHOOL

MONTEREY, CALIFORNIA

THESIS

IN-SERVICE INSPECTION APPROACHES FOR LEAD-COOLED NUCLEAR REACTORS

by

James C. Bowen

June 2017

Thesis Advisor: Craig F. Smith
Second Reader: James H. Luscombe

Approved for public release. Distribution is unlimited.

THIS PAGE INTENTIONALLY LEFT BLANK

REPORT DOCUMENTATION PAGE			Form Approved OMB No. 0704–0188
Public reporting burden for this collection of information is estimated to average 1 hour per response, including the time for reviewing instruction, searching existing data sources, gathering and maintaining the data needed, and completing and reviewing the collection of information. Send comments regarding this burden estimate or any other aspect of this collection of information, including suggestions for reducing this burden, to Washington headquarters Services, Directorate for Information Operations and Reports, 1215 Jefferson Davis Highway, Suite 1204, Arlington, VA 22202-4302, and to the Office of Management and Budget, Paperwork Reduction Project (0704-0188) Washington, DC 20503.			
1. AGENCY USE ONLY ***(Leave blank)***	**2. REPORT DATE** June 2017	**3. REPORT TYPE AND DATES COVERED** Master's thesis	
4. TITLE AND SUBTITLE IN-SERVICE INSPECTION APPROACHES FOR LEAD-COOLED NUCLEAR REACTORS		**5. FUNDING NUMBERS**	
6. AUTHOR(S) James C. Bowen			
7. PERFORMING ORGANIZATION NAME(S) AND ADDRESS(ES) Naval Postgraduate School Monterey, CA 93943-5000		**8. PERFORMING ORGANIZATION REPORT NUMBER**	
9. SPONSORING /MONITORING AGENCY NAME(S) AND ADDRESS(ES) N/A		**10. SPONSORING / MONITORING AGENCY REPORT NUMBER**	
11. SUPPLEMENTARY NOTES The views expressed in this thesis are those of the author and do not reflect the official policy or position of the Department of Defense or the U.S. Government. IRB number ____N/A____.			
12a. DISTRIBUTION / AVAILABILITY STATEMENT Approved for public release. Distribution is unlimited.		**12b. DISTRIBUTION CODE**	

13. ABSTRACT (maximum 200 words)

Lead-cooled fast reactors (LFRs) present design challenges in accomplishing in-service inspections (ISIs) due to the opacity, corrosiveness, and high operating temperature of lead. Current technology can adjust to accomplish ISIs for LFRs. The inspections identified and outlined in this thesis are intended to address Nuclear Regulatory Commission requirements for advanced reactor design concerning ISIs.

This research identifies ISI requirements for advanced reactors such as the LFR, assesses current ISI techniques on functioning and proposed reactors, and tests the physics theory, ensuring compatibility with LFRs. Techniques evaluated were considered applicable to LFRs, and in general, require further development. Acoustic, thermal, and eddy-current testing methods were individually evaluated for use in an LFR and compared to the operating conditions of functioning and proposed reactors. Each method was found to be potentially feasible for application to ISI of LFRs based on the consideration of basic physics theory. Overall, this thesis provides an outline of technologies that can accomplish ISIs, making LFRs a more viable option for meeting future energy demands.

14. SUBJECT TERMS in-service inspections, lead-cooled nuclear reactors, acoustic attenuation, eddy-current testing			**15. NUMBER OF PAGES** 93
			16. PRICE CODE
17. SECURITY CLASSIFICATION OF REPORT Unclassified	**18. SECURITY CLASSIFICATION OF THIS PAGE** Unclassified	**19. SECURITY CLASSIFICATION OF ABSTRACT** Unclassified	**20. LIMITATION OF ABSTRACT** UU

NSN 7540–01-280-5500 Standard Form 298 (Rev. 2–89)
Prescribed by ANSI Std. 239–18

THIS PAGE INTENTIONALLY LEFT BLANK

Approved for public release. Distribution is unlimited.

IN-SERVICE INSPECTION APPROACHES FOR LEAD-COOLED NUCLEAR REACTORS

James C. Bowen
Captain, United States Army
B.S., United States Military Academy, 2007

Submitted in partial fulfillment of the
requirements for the degree of

MASTER OF SCIENCE IN PHYSICS

from the

NAVAL POSTGRADUATE SCHOOL
June 2017

Approved by: Craig F. Smith
Thesis Advisor

James H. Luscombe
Second Reader

Kevin B. Smith
Chair, Department of Physics

THIS PAGE INTENTIONALLY LEFT BLANK

ABSTRACT

Lead-cooled fast reactors (LFRs) present design challenges in accomplishing in-service inspections (ISIs) due to the opacity, corrosiveness, and high operating temperature of lead. Current technology can adjust to accomplish ISIs for LFRs. The inspections identified and outlined in this thesis are intended to address Nuclear Regulatory Commission requirements for advanced reactor design concerning ISIs.

This research identifies ISI requirements for advanced reactors such as the LFR, assesses current ISI techniques on functioning and proposed reactors, and tests the physics theory, ensuring compatibility with LFRs. Techniques evaluated were considered applicable to LFRs, and in general, require further development. Acoustic, thermal, and eddy-current testing methods were individually evaluated for use in an LFR and compared to the operating conditions of functioning and proposed reactors. Each method was found to be potentially feasible for application to ISI of LFRs based on the consideration of basic physics theory. Overall, this thesis provides an outline of technologies that can accomplish ISIs, making LFRs a more viable option for meeting future energy demands.

THIS PAGE INTENTIONALLY LEFT BLANK

TABLE OF CONTENTS

LIST OF FIGURES

LIST OF TABLES

THIS PAGE INTENTIONALLY LEFT BLANK

LIST OF ACRONYMS AND ABBREVIATIONS

ARDC	Advanced Reactor Design Criteria
BWR	Boiling Water Reactor
DLFR	Demonstration Lead-cooled Fast Reactor (Westinghouse)
DoE	Department of Energy
DOD	Department of Defense
ECT	Eddy-Current Testing
ELSY	European Lead-cooled System
EMP	Electro-Magnetic Pulse
Gen-IV	Generation IV
GIF	Generation IV International Forum
IEMA	Illinois Emergency Management Agency
ISI	In-Service Inspection
LBE	Lead-Bismuth Eutectic
LFR	Lead-cooled Fast Reactor
LWR	Light-Water Reactor
NRC	Nuclear Regulatory Commission
PNNL	Pacific Northwest National Lab
PWR	Pressurized Water Reactor
RPV	Reactor Pressure Vessel
RTD	Resistance Temperature Detector
RV	Reactor Vessel
SFR	Sodium-cooled Fast Reactor
SG	Steam Generator
SPIDERS	Smart Power Infrastructure Demonstration for Energy Reliability and Security
SSTAR	Small, Sealed, Transportable, Autonomous Reactor

THIS PAGE INTENTIONALLY LEFT BLANK

ACKNOWLEDGMENTS

First, I want to first thank my thesis advisor, Dr. Craig Smith. His expertise in nuclear engineering and passion for developing future energy production changed me from an interim student to a lifetime academic and amateur researcher. Without his depth of knowledge, connections in the field, and hours on the phone, my thesis would still be an outline with a few cool pictures. I'm thankful for his willingness to educate me and look forward to our continuing friendship.

Second, I want to thank the faculty and staff of the Physics Department at the Naval Postgraduate School. The faculty's treatment of students as fellow researchers and future co-workers fueled my drive to reach beyond the requirements of my degree. I would like to specifically thank Dr. James Luscombe and Dr. Bruce Denardo, who put up with my edits and questions, which occasionally led classes off-topic during the last two years. They helped me focus and work toward becoming a future educator.

Last, I want to thank my family. I have an amazing support network and a great team. My parents' continued guidance inspires me to accomplish what I can to make them proud. My sister and her family continue to cheer on my efforts with small and endearing reminders. My parents-in-law provide continuous support to my family and encouragement to me in my work, and I am thankful for both. The inquisitive nature of my children, Zoie and Andrew, continues to help me look at everything as if for the first time. I love you all and am happy to be so blessed. Finally, without my wife following me around the country, I'd never be able to pursue my dreams of becoming an officer, teacher, and father at the same time. Her support means the most, and I look forward to continuing our adventure in the Army, academia, and wherever we go next.

THIS PAGE INTENTIONALLY LEFT BLANK

I. INTRODUCTION

A. MOTIVATION

Despite growing demand and increasing restrictions on fossil fuels, there is a technology gap for reliable, safe and non-carbon electrical energy sources in the world. The near-term implication of this gap is increased reliance on sources that are unreliable or environmentally unfriendly to meet both civilian and military demands. The energy gap on the military side includes not only reliance on the civilian electric grid but also the use of generators for field operations and for backup electricity in case of grid failure. These generator systems are noisy and require frequent maintenance and fuel resupply in addition to their reliability and environmental drawbacks. Renewables such as solar and wind power are dependent on the natural environment and therefore not attainable in all regions, and not dependable where they are available due to their intermittency. Hydroelectric power is also not available everywhere, generally requires major resource development (dam building, etc.), and affects the ecosystems surrounding the power plant. Current gas/coal power generation puts a strain on the environment through release of carbon dioxide and other pollutants to the atmosphere, and requires constant re-supply of natural resources. Even modern nuclear power plants have drawbacks, including public skepticism due to high-profile accidents affecting large-scale regions and the concerns related to disposal of nuclear waste.

The Generation IV (Gen-IV) initiative was established in 1995 to explore a new generation of advanced nuclear power technologies to overcome many of the past concerns with nuclear energy. Currently, the Gen-IV International Forum (GIF) is tasked with coordinating international design efforts for next-generation nuclear reactors to meet future energy requirements (OECD/NEA 2014). Of the reactor technologies identified to date, the lead-cooled fast reactor (LFR) is a promising candidate to meet the technology gap mentioned above in the United States and globally. The inherent properties of lead make the LFR able to operate at temperatures well below the boiling temperature producing electricity with high efficiency while the coolant remains near atmospheric pressure. This allows engineers to scale the LFR to meet the needs of the energy sector.

Lead also provides an excellent shield against gamma radiation, and lead-cooled reactors are expected to have economic advantages compared to other nuclear coolant/moderator systems due to design simplifications enabled by the natural properties of lead. The scalability and inherent safety of LFR designs indicate a good potential that they can meaningfully contribute to meeting the energy requirements of the United States, and the military's need for reliable fixed station and deployable power (see Appendix H).

B. PROBLEM STATEMENT

One of the challenges in the development of the LFR is the lack of developed technology to conduct in-service inspections. The opacity, high operating temperature and corrosiveness of molten lead present the main challenges to inspecting internal components of LFRs. The research goals of this thesis are to identify the requirements for in-service inspection (ISI), evaluate the critical components of current liquid metal cooled designs, summarize how those components could fail under normal operations, and propose inspection methods to meet regulatory requirements while minimizing the potential for failure.

C. RESEARCH QUESTIONS

The research questions to be addressed in confronting this problem are the following:

- What are the in-service inspection requirements for lead-cooled fast reactors?
- Is there current technology used on other reactors that can satisfy inspection requirements for lead cooled fast reactors?
- Can we apply ultrasonic, thermal, or imagery diagnostics being developed for use on sodium-cooled reactors to lead-cooled reactors?
- Do current methods for conducting out-of-service inspections on lead-cooled reactors provide a viable alternative?

D. METHODS AND SCOPE

The research for this thesis consists of three segments. First is the identification of inspection requirements for lead-cooled fast reactors or other similar advanced reactors.

Next is the determination of the critical components requiring inspection based on those requirements. Finally, for each component, the research assesses both technologies currently used on other reactor systems, and possible applications of additional technologies, not currently being regularly implemented, to determine appropriate approaches to inspection.

The goal of this study is to determine the best way forward for inspecting reactor components in LFRs. The thesis will primarily cover properties of current designs of lead-cooled fast reactors. From those design specifications, the research will apply physics theory and mathematical analysis to evaluate the potential of the identified ISI technology approaches. The scope of this effort is limited to initial evaluation of typical reactor parameters to ensure that current technical approaches identified for LFRs and other advanced reactor systems can be applied to the LFR. Our research is not meant to fully develop new inspection technologies beyond initial research and consideration of future possible applications. The scope of this project also does not include response to external factors such as natural disasters, and instead focuses on challenges anticipated during normal operations of the reactor systems.

Following this introduction, Chapter II discusses the background information to develop LFRs. It includes general design specifications, design challenges, and current technology used on other reactor designs for ISI. Chapter III addresses the methodology used in determining required inspections and the physics behind current ISI techniques. Chapter IV describes the results obtained by applying physics theory of currently used ISI to a general LFR reactor design. Chapter V presents the summary, conclusions, and recommendations for future research. The appendices include the equations, computer coding, and an overview of LFR applications.

THIS PAGE INTENTIONALLY LEFT BLANK

II. BACKGROUND

A. LEAD-COOLED FAST REACTORS

Nuclear reactors are complex systems containing, at their heart, materials capable of undergoing self-sustaining, controlled nuclear fission to generate heat. This heat is converted into mechanical and then electrical energy by transferring heat (usually through a steam generator) into steam which drives a turbine generator, producing electricity. Nuclear reactors generally fall into two categories: thermal reactors and fast neutron reactors or "fast reactors" for short. Thermal reactors use coolants with relatively low atomic mass that act as a good moderator with a high scattering cross section to slow down or "thermalize" high-energy neutrons that emerge from the fission process. This slowing process is called thermalization, which lowers the neutron energy through collisions with the moderator. The fuel is designed to absorb these low energy thermalized neutrons with a high probability so that additional fissions can take place and the fission process can be sustained. A sketch of a thermal reactor of the Pressurized Water Reactor (PWR) type is shown below.

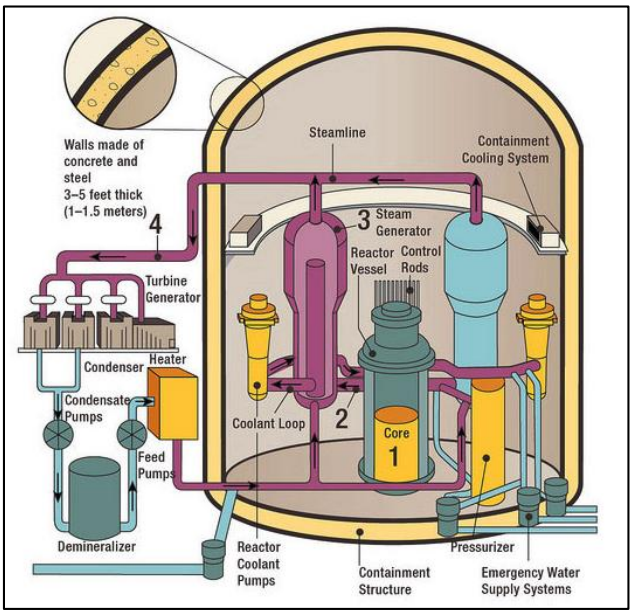

Figure 1. Pressurized Water Reactor Sketch. Source: U.S. NRC (2015).

Fast reactors take a different approach: they use the fast neutrons caused by fission more directly to create successive fission reactions. In this case, the fuel is arranged in such a way as to absorb neutrons that have maintained their high energy (i.e., fast neutrons). The coolant is chosen to be a poor moderator to allow neutrons to maintain their energy. These high-energy neutrons react with the reactor fuel to induce subsequent fissions and thereby produce additional fission energy and fast neutrons. The fuel is chosen to enhance absorption of these high-energy neutrons to allow subsequent fission reactions (Department of Energy, 1993). A sketch of the European Lead-cooled SYstem (ELSY) is shown below as an example of a demonstration LFR in the design phase.

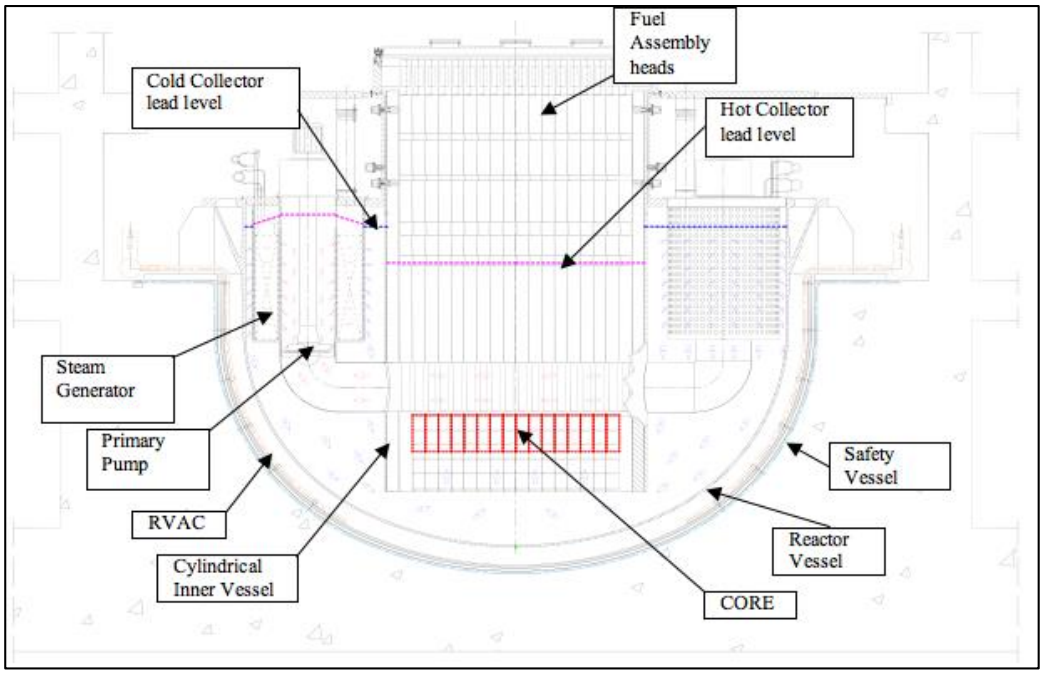

Figure 2. ELSY Sketch. Source: Smith and Cinotti (2016).

Lead and Lead-Bismuth Eutectic alloy (LBE) are two choices the Generation IV International Forum (GIF) considers for the coolant in heavy liquid metal fast reactor technology (OECD/NEA, 2014). Both have low energy loss in scattering (i.e., poor moderation due to the heavy mass of the coolant atoms) and low neutron absorption making them efficient coolants in fast reactors. Both have manageably low melting points (124ºC for LBE, 327ºC for lead) and very high boiling points (1670ºC for LBE, 1737ºC

for lead) making them stable and not subject to boiling at the typical operating temperatures of 5–600°C (GIF LFR pSSC, 2015). They have low vapor pressures making them operable at near atmospheric pressure. Both are relatively inert when in contact with air or water making them safe choices for a coolant (Smith and Cinotti, 2016). Because of the physical and chemical properties of lead and LBE, reactors cooled by these materials are expected to be scalable, efficient, and intrinsically safe.

B. LFR DESIGN CHALLENGES AND SPECIFICATIONS

There are a few drawbacks of lead and LBE as coolants. These materials are opaque, which makes monitoring and inspection of internal components a challenge. The coolants are also very heavy, making the challenge of containment and protection against structural damage (e.g., under seismic mechanical loads) an additional problem. Lead and LBE are also corrosive to conventional steels at high temperatures. In contrast to lead, LBE is much more expensive, and produces polonium-210 through neutron capture in the bismuth. According to Smith and Cinotti (2016), "^{210}Po decays with a half-life of 138.4 days into ^{206}Pb by an α emission of 5.3 MeV. Therefore, it represents a potent heat load within the coolant as well as being a dangerous and radiotoxic material in the event of its leakage or release." Overall, these drawbacks represent important challenges, but the benefits of lead as a coolant are also substantial and enable innovation in reactor design, including inspection techniques.

There are several LFRs in the design and construction phases with common characteristics due to lead properties. Because of the opacity and density of lead, most focus on a pool-type configuration, and several feature removable components for periodic inspection. The coolant flow moves lead through the core where it is heated, then to a steam generator (SG) or other heat exchange mechanism by pumping or natural circulation, and finally following flow channels in the reactor vessel (RV) back to the core. The SGs and RV are common to other pool-type nuclear reactor designs. LFRs range in size from the small systems such as the Small Sealed Transportable Autonomous Reactor (SSTAR) at a projected 20 MWe to the larger central-station European Lead Fast Reactor projecting 600 MWe output (Smith and Cinotti, 2016). Smaller systems have

also been envisioned (e.g., SEALER at 3–10 MWe) as have larger ones (e.g., BREST-1200 at 1200 MWe).

Because LFRs are mostly in the design phase, the dimensions and materials are seldom fully detailed. There are two reactors for which design specifications have been published in a form that is readily usable for this research. The two reactors – ELSY and the Westinghouse Demonstration LFR – are summarized below.

The ELSY is an earlier design of a European LFR reactor. Listed in Table 1 are the basic parameters of ELSY. Based on the dimensions in this parameter listing, and comparing to the schematic shown previously in Figure 2, the ELSY size and temperature specifications have been used for the assessments in this thesis. From the information in this table and figure, the reactor vessel is taken to be approximately 11.5m in diameter, the distance from the base of the reactor vessel to the core is taken at 1.5m, and the depth of the top of the core from the free lead level is taken at 5.75m.

Table 1. ELSY Parameters. Source: Tarantino, Cinotti, and Rozzia (2012).

Parameter	ELSY
Power, MWth	1500
Thermal efficiency, (%)	42
Primary coolant	Lead
Primary coolant circulation (at power)	Forced
Core inlet temperature, (°C)	400
Core outlet temperature, (°C)	480
Fuel	MOX, (Nitrides)
Peak cladding temperature, (°C)	550
Fuel pin diameter, (mm)	10.5
Active core dimensions Height/equivalent diameter, (m)	0.9/4.32
Power conversion system working fluid	Water-superheated steam at 18 MPa, 450°C
Primary/secondary heat transfer system	Eight Pb-to-H2O SGs
Fuel column height. (mm)	900
N° Fuel Assemblies (FA)	162
FA geometry	Open square
FA pitch, (mm)	294
N° fuel pins / FA	428
Fuel pins pitch (at 20°C, (mm)	13,9 square
Fuel pins outer diameter, (mm)	10,5
Enrichment, (%wHM)	14.54/17.63/20.61 Pu, three radial zones

The second design example is based on the published information of the Westinghouse Demonstration LFR (Westinghouse Electric Company, LLC., 2016) which includes many of its material, temperature, and flow rate specifications. This design is similar in some ways to ELSY, and is a shorter pool-type reactor with integrated steam generation power production and heat removal system.

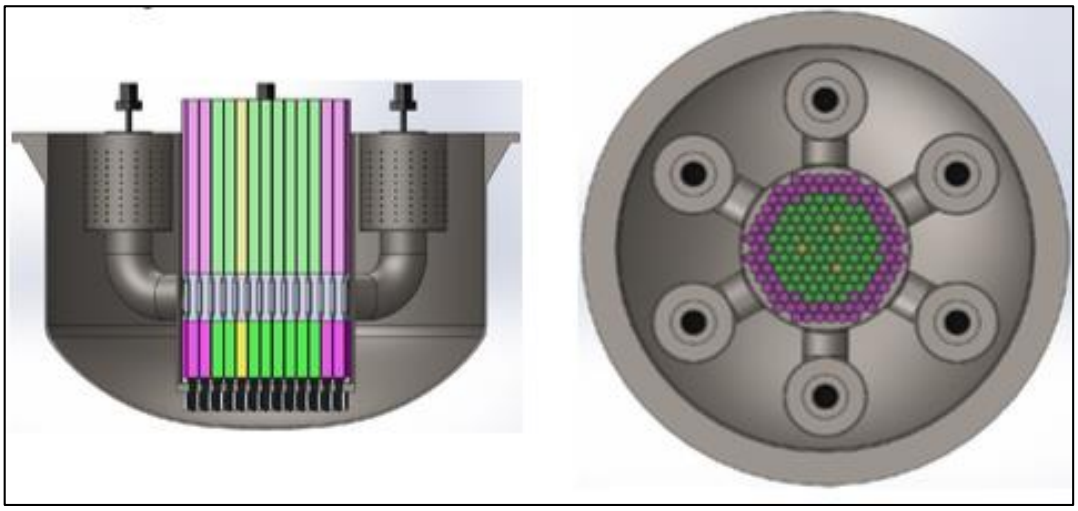

Figure 3. Westinghouse DLFR Sketch. Source: Westinghouse Electric Company (2016).

Westinghouse has refined and tested the materials to be deployed in their demonstration reactor under operating conditions. Their material development and status are shown in Table 2. The Westinghouse LFR plant characteristics are shown in Table 3.

Table 2. Technology Readiness Level for Materials Envisaged for Key DLFR Components. Source: Westinghouse Electric Company, LLC. (2016).

Material	Component	Status	TRL
UO_2	Fuel	Fully tested and qualified for fast reactors	9
D9	Whole assembly structure, including fuel rod cladding	Fully tested and qualified for fast reactors (currently used in the FBTR in India [16])	9
Al_2O_3	Coating[a] (for components exposed to Pb at T>~450°C)	Tested in lead up to 600 °C [1]. Irradiated with heavy ions (up to 150 dpa on D9 [2], up to 450 dpa on 316L [3])	5
AISI 316(L)	Inner Vessel, Lower core plate, Main Vessel, Internals, SG tubes[b]	Tested in lead	8
AISI 400 series	Pump impeller	To be tested – coated – in pool configuration and representative conditions	4

[a] Al_2O_3 is the reference coating material. Other coating options are also being tested (e.g. FeCrAl).
[b] Other material options, such as SS347 or SS304H, are also under consideration for the SG tubes.

Table 3. Summary of DLFR Plant Characteristics. Source: Westinghouse Electric Company, LLC. (2016).

Power- and cycle length-related related characteristics			
Power (thermal/electric)	Phase I	MW	500/210
	Phase II		Up to 700/340
Plant net efficiency	Phase I	%	42.0
	Phase II		46-48
Core average power density		kW/l	102
Peak power density		kW/l	149
Cycle length		mo	18
Fuel residence time		EFPM	108
Peak fast neutron flux		n/cm^2 s	$1.81x10^{15}$
Primary system operating conditions			
Pressure		MPa	~0.1
Core inlet temperature		°C	390
Core outlet temperature		°C	510
Lead mass flow rate		kg/s	28560
Lead volumetric flow rate		m^3/s	2.74
Average lead velocity in the core		m/s	1.41
Core characteristics			
Core diameter (incl. shield assemblies)		m	4.3
Number of assemblies (fuel+safety+shield)		-	163
Number of fuel assemblies (inner/outer region)		-	82 (34/48)
Number of shield assemblies		-	78
Number of safety assemblies		-	3
Fuel assembly lattice		-	Hex, with duct
Fuel rod support type		-	Grids
Assembly pitch		mm	304
Assembly side-to-side distance (outer/inner)		-	301/296
Central beam tube ID		mm	78
Fuel rods per assembly		-	432
Fuel rod pitch		mm	13.6
Fuel rod OD		mm	11.6
P/D		-	1.17
Fuel rod cladding thickness		mm	0.65
Fuel pellet diameter (outer/inner)		mm	10.0/3.0
Fuel pin total length		mm	1530
Fueled length		mm	700
Plenum length		mm	600
Fuel and materials			
Fuel material		-	UO_2
Fresh fuel enrichment (inner/outer)		%	17.5/19.9
Heavy Metal mass		MT	16.26
Discharge burnup (average/peak)		MWD/kg_{HM}	100/140
Feed assemblies per year		-	9.1
Structural materials		-	See Table 4
Secondary system characteristics			
Pressure		MPa	18
Feedwater temperature at SG inlet		°C	340
Steam temperature at SG outlet		°C	500
Number of SGs		-	6

C. CURRENT INSPECTION TECHNOLOGY

This research takes advantage of current technology developed for use in Sodium-cooled fast reactors (SFRs), and various functioning water/steam cooled reactor systems. The transducer designs, reactor vessel inspection techniques, steam generator inspection methods, current temperature sensors, and filtration techniques that could potentially be used for molten lead systems are described below. These methods and designs outline the technologies applied to our specific LFR designs to check for compatibility. Additionally, they rule out need for further development in techniques that are not appropriate to an LFR design.

1. Ultrasound in SFRs

There are several methods to conduct acoustic evaluation in a medium. Designers of SFRs are currently developing technology to use piezo-electric ultrasonic transducers to conduct ISI (PNNL, 2009). Pacific Northwest National Laboratory identified seven different countries with ongoing research in transducer design for use in an SFR. The general design is shown below and has been successfully tested in water.

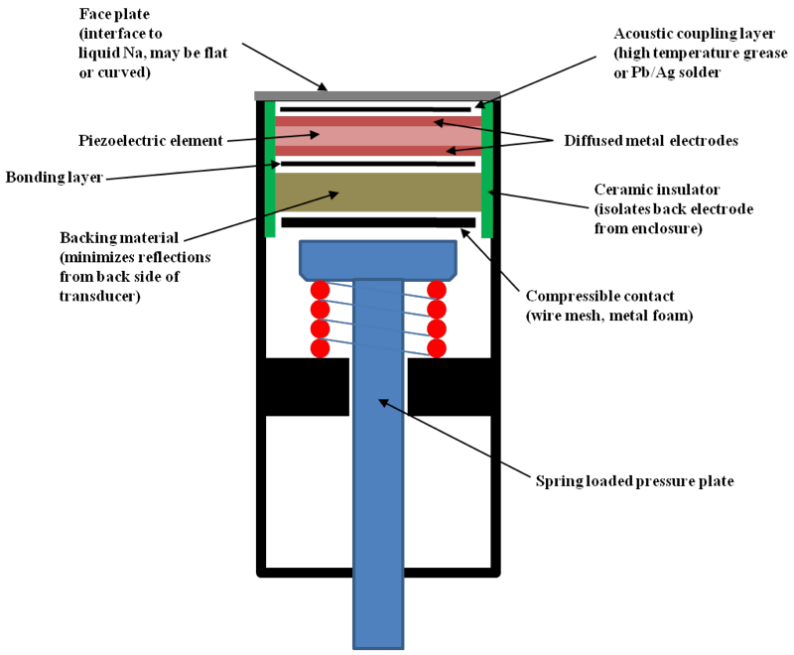

Figure 4. Basic Transducer Design. Source: PNNL (2009).

These transducers act as a single transducer or in an array, as transmitters and receivers to emit and receive pressure waves that are converted to an alternating voltage. These multiple voltage readings are calibrated to display an image. At PNNL, their transducer emitted an ultrasonic pulse at 5MHz in water and received adequate signal response to get a 2D image of their specified object (PNNL, 2009). The array is meant to sit at the bottom of the reactor vessel to get a bottom-up picture of the core.

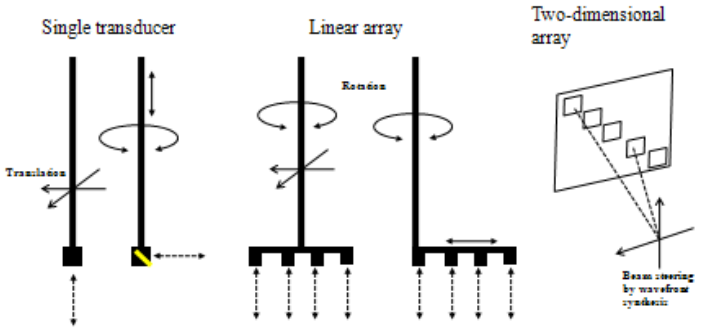

Figure 5. Array Configurations for Ultrasonic Testing. Source: PNNL (2009).

With a ½" diameter transducer, PNNL managed to get 0.01" resolution in water. Although conducted in water, the acoustic impedance is within an order of magnitude of that of sodium, so the resolution would be expected to be similar.

2. ISI on Reactor Vessels

There is current extensive probing done in pressurized water reactors and boiling water reactors to verify integrity of the reactor pressure vessel (RPV). Systems work both inside and outside of the RPV using visual imagery, ultrasound, and eddy-current testing. The RPV-ISI Tool outlined in the European Conference on Non-Destructive Testing in 2010 is on a large harness, constantly moving and scanning (Pajnić et al., 2010). It has cameras for visual inspection, ultrasonic sensors for acoustic sensing, and eddy-current probes for electrical testing.

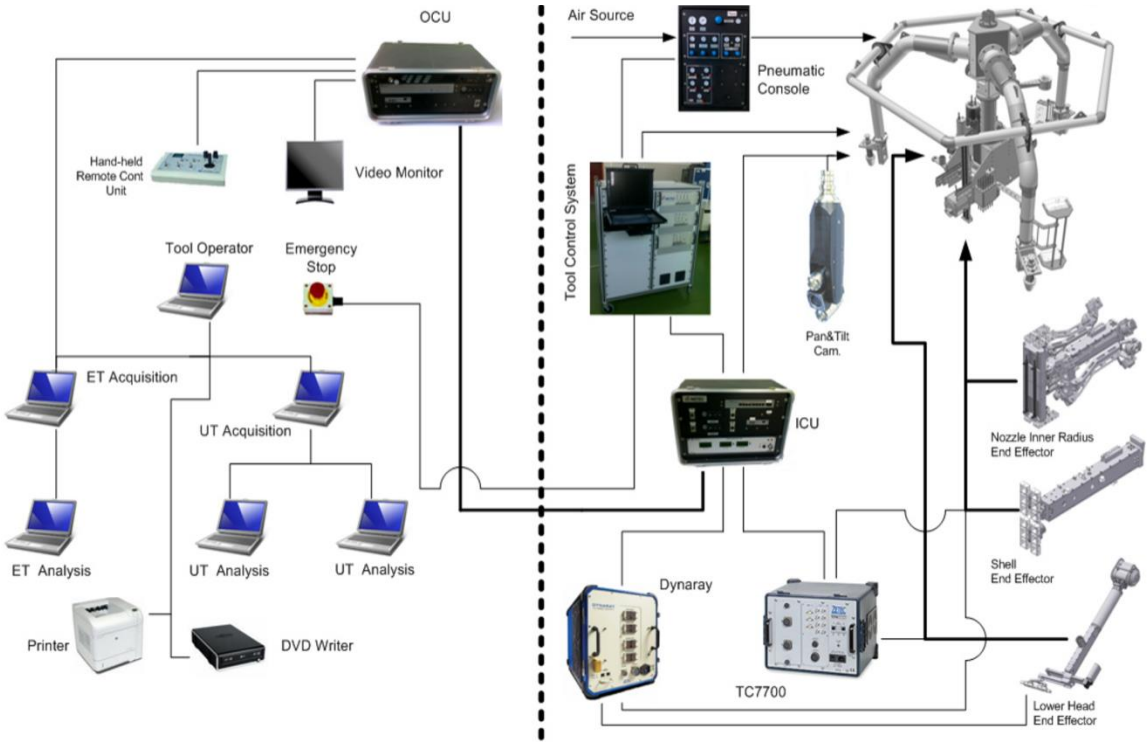

Figure 6. Electrical Layout of the RPV-ISI Tool. Source: Pajnić et al. (2010).

The ultrasonic transducers in the RPV-ISI Tool operate to detect flaws up to 40mm in depth, while the eddy-current testing (ECT) feature can detect subsurface flaws at a higher confidence but only to 2.5mm in depth (Pajnić et al., 2010). The visual inspections of the RPV-ISI Tool can detect surface defects larger than 0.8mm in width. The overall system can accommodate up to 12 sensors of either type to conduct simultaneous scanning. This system meets all NRC requirements for ISI of the reactor pressure vessel to ensure safe operating conditions.

3. Steam Generator Inspections

Currently, nuclear reactors, steam generators and heat exchangers are probed periodically to detect corrosion conditions through eddy-current testing or ultrasonic probing. Because piezo-electric ultrasonic testing was discussed previously, ECT is discussed further here. ECT is a proven method of exploiting the electromagnetic properties of the material inspected to detect irregularities or flaws in the material. One

company specializing in such technology is BWXT, which deploys the ZR-100 robot to inspect and repair steam generators and heat exchangers (BWXT, 2017).

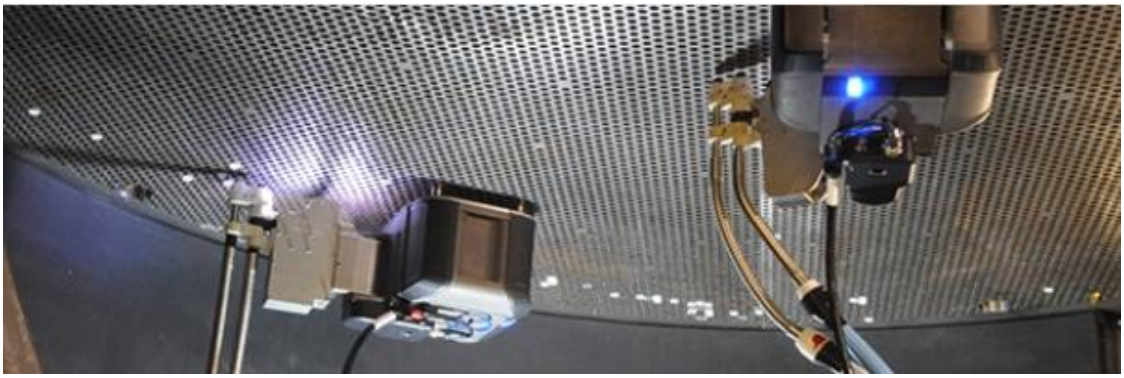

Figure 7. ZR-100 Robot. Source: BWXT (2017).

These inspections are conducted autonomously by the robot and "the ZR-100 can access over 200 tubes from a single stance, and can traverse the tube sheet at speeds of 5 feet per minute" (BWXT, 2017). Because the robot has to be in close proximity to the inspected component, inspections are conducted during scheduled service outages in the nuclear reactor. These are conducted during full reactor shutdown or on a rotational basis. The robot has a self-contained ECT head, which probes and detects flaws along the steam generator tubes.

4. Temperature Sensing

Two main types of temperature sensors are used in thermal sensing inside nuclear reactors: resistance temperature detectors (RTDs) and thermocouples. RTDs use wire wrapped around a ceramic or glass core, which changes resistance as temperature changes (Jethra, 2013). They are extremely sensitive, but are therefore unstable in high vibration settings. They also are more expensive than thermocouples. Thermocouples measure a voltage from the joining of two distinct metals when heated. The voltage is calibrated to get a temperature reading. Thermocouples are better in high temperature and high vibration environments (Jethra, 2013).

5. Filtration of Lead

To inspect the condition of liquid metal coolants, current methods rely on periodic testing at the filtration devices. In addition to monitoring the coolant itself, these filtrates can provide information related to the corrosion or erosion processes affecting components in contact with the coolant. There are commercially available ceramic honeycomb filters. The company Induceramic makes an Al_2O_3 based filter specified below:

Table 4. Ceramic Honeycomb Filter Specifications.
Source: Induceramic (2017).

Material	Al_2O_3 (%)	Channel Shape	Pore Size (μm)	Coefficient of Thermal Expansion ($\times 10^{-6}/^0C$)	Softening Temperature (^0C)	Compressive Strength at 25 ^0C (MPa)
Cordierite	37	round/square	2~3	≤1.8	1390	≥12
Mullite	46		2~3	≤4.0	1550	≥15
Corundum-mullite	70		2~3	≤5.5	1700	≥15

Filter channel sizes range from 1.5-3mm and the filters are either round or square in cross section, which reduces turbulence with molten lead passing through (Induceramic, 2017).

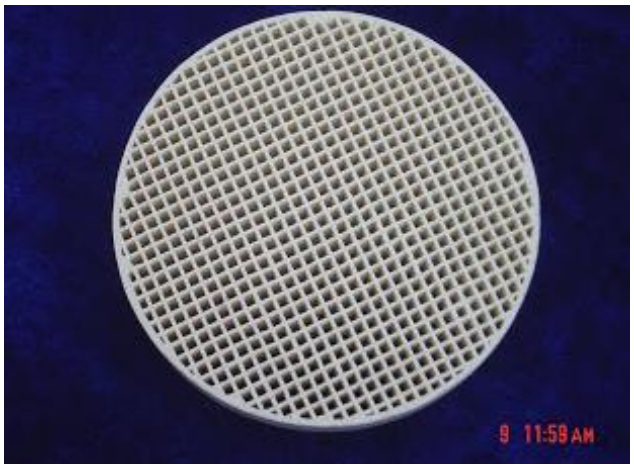

Figure 8. Image of Ceramic Honeycomb Filter. Source: Induceramic (2017).

Although previously used primarily in metallurgical operations, this filter type provides a method in which to inspect for corrosion and radioactive material buildup through the steam generators in lead cooled reactors.

THIS PAGE INTENTIONALLY LEFT BLANK

III. METHODOLOGY

Current technology is available to accomplish in service inspections of lead-cooled fast reactors to meet the general design criteria for nuclear power plants. To ensure all design criteria are met, these inspections would be accomplished through continuous and periodic means. The first step of our research is to identify inspections suited for an LFR based on regulatory design criteria. The United States Nuclear Regulatory Commission (NRC) has several general design criteria for nuclear power plants, focusing on Light-water reactors (LWRs), and has recently drafted new design criteria for Advanced Reactors (US NRC, 2017). Because LFRs are not fully developed in the United States, these more recently drafted criteria were used as a baseline.

A. NRC DESIGN CRITERIA

The NRC Advanced Reactor Design Criteria (ARDC) in its draft form outline eight inspection criteria as specified tasks (US NRC, 2017). They are listed in Table 5.

Table 5. Applicable NRC Design Criteria for ISI. Source: U.S. NRC (2017).

Criterion	ARDC Title and Content
18	*Inspection and testing of electric power systems.* Electric power systems important to safety shall be designed to permit appropriate periodic inspection and testing of important areas and features, such as wiring, insulation, connections, and switchboards, to assess the continuity of the systems and the condition of their components. The systems shall be designed with a capability to test periodically (1) the operability and functional performance of the components of the systems, such as onsite power sources, relays, switches, and buses, and (2) the operability of the systems as a whole and, under conditions as close to design as practical, the full operation sequence that brings the systems into operation, including operation of applicable portions of the protection system, and the transfer of power among systems.
21	*Protection system reliability and testability.* The protection system shall be designed for high functional reliability and inservice testability commensurate with the safety functions to be performed. Redundancy and independence designed into the protection system shall be sufficient to assure that (1) no single failure results in loss of the protection function and (2) removal from service of any component or channel does not result in loss of the required minimum redundancy unless the acceptable reliability of operation of the protection system can be otherwise demonstrated. The protection system shall be designed to permit periodic testing of its functioning when the reactor is in operation, including a capability to test channels independently to determine failures and losses of redundancy that may have occurred.
32	*Inspection of reactor coolant boundary.* Components that are part of the reactor coolant boundary shall be designed to permit (1) periodic inspection and functional testing of important areas and features to assess their structural and leak tight integrity, and (2) an appropriate material surveillance program for the reactor vessel.
36	*Inspection of emergency core cooling system.* A system that provides emergency core cooling shall be designed to permit appropriate periodic inspection of important components to ensure the integrity and capability of the system.
42	*Inspection of containment atmosphere cleanup systems.* The containment atmosphere cleanup systems shall be designed to permit appropriate periodic inspection of important components, such as filter frames, ducts, and piping to assure the integrity and capability of the systems.
45	*Inspection of structural and equipment cooling systems.* The structural and equipment cooling systems shall be designed to permit appropriate periodic inspection of important components, such as heat exchangers and piping, to ensure the integrity and capability of the systems.
53	*Provisions for containment testing and inspection.* The reactor containment structure shall be designed to permit (1) appropriate periodic inspection of all important areas, such as penetrations, (2) an appropriate surveillance program, and (3) periodic testing at containment design pressure of the leak- tightness of penetrations that have resilient seals and expansion bellows.
64	*Monitoring radioactivity releases.* Means shall be provided for monitoring the reactor containment atmosphere, effluent discharge paths, and plant environs for radioactivity that may be released from normal operations, including anticipated operational occurrences, and from postulated accidents.

With further refinement, these eight design criteria can be grouped into four subcategories. Four inspection criteria groups are further addressed:

- Inspection of general system functions (ARDC Criteria 18, 21)
- Inspection of component integrity (ARDC Criteria 21, 32, 42, 45, 53)
- Inspection of coolant characteristics and boundaries (ARDC Criteria 21, 32, 36, 45, 53)
- Inspection of atmospheric cleanup and radioactive release control (ARDC Criteria 42, 64)

B. CRITICAL COMPONENTS/FAILURE OPPORTUNITIES

For each focused design criteria group, the first step is to identify the critical components for pool-type LFRs. Most failure opportunities for normal operations in a LFR involve one of five categories: General electrical failure, corrosion from molten lead interaction with materials, rupture or break of components, coolant blockage, or change in coolant chemistry. The critical inspections by design criteria group are

- Inspection of general system functions: Electrical systems and steam generators.
- Inspection of component integrity: Steam generators, core assembly, and reactor vessel.
- Inspection of coolant characteristics and boundaries: Coolant flow and chemistry.
- Inspection of atmospheric cleanup and radioactive release: General atmospheric conditions outside reactor.

In general, to meet NRC design criteria, the research dictates inspection of atmospheric conditions, general electrical systems, coolant, core assembly, reactor vessel, and steam generators. The specific inspections and design criteria that they satisfy are identified in the following paragraphs.

1. Atmospheric Conditions

The monitoring of atmospheric conditions surrounding a reactor is already heavily regulated and mature. For example, the Illinois Emergency Management Agency (IEMA) conducted 805 soil samples testing for radionuclides around their six nuclear reactors in

2015 (IEMA, 2016, 3). In addition, they currently have 1649 environmental dosimeters testing for gamma radiation inside and deployed in 10-mile radius around their nuclear reactors (IEMA, 2016, 3). The testing is extensive, periodic, and sufficient to satisfy ARDC Criteria 42 and 64 for atmospheric testing outside of nuclear reactors. Because of this, the monitoring of atmospheric conditions will not be further developed in this research.

2. General Electrical Systems

The general electrical framework of the reactor must be inspected to meet ARDC Criteria 18 and 21. This requires no special inspections unique to LFRs, and only general electrical testing. Because of this, it will not be further developed in this research.

3. Coolant

Because the coolant in an LFR provides a significant degree of inherent radiation protection and, additionally, is critical in providing both operational and emergency cooling, it requires several inspections. The free lead level requires inspection to ensure proper function of the coolant circulation systems, meeting Criterion 45. Because there is an air gap above the free lead level, it can be inspected by camera and nothing further is required. The chemical condition of the lead requires periodic inspection ensuring no fission product buildup and no component corrosion or erosion meeting Criteria 32 and 45. This can be done at the filtration system in the steam generator, which also requires no further physics to develop. The temperature of the coolant needs to be carefully monitored to ensure its function as a coolant and proper lead flow in meeting ARDC Criteria 21, 36, and 45.

4. Core Assembly

The core contains components essential for heat generation and reactivity control. The individual components ensure general reactor functions. Because of this, inspection of component integrity meets Criteria 32, 45, and 64. Additionally, temperature inspections inside the core are required to ensure the core cooling system, including emergency core cooling, is working properly, meeting Criterion 36.

5. Reactor Vessel

The reactor vessel is susceptible to corrosion due to the properties of molten lead. The integrity of the reactor vessel therefore requires periodic inspections of the welds holding the reactor vessel together and of the vessel itself. This meets Criteria 21, 32, and 53.

6. Steam Generators

Steam generator component integrity requires periodic inspection to ensure absence of corrosion for parts in contact with the coolant. This meets Criterion 32. Additionally, the general integrity of the steam generator meets Criteria 21 and 45, which concern the cooling and protection systems of the reactor.

C. ACTUAL DESIGN TESTING

The first part of the ISI design assessment of this thesis was to conduct thorough research into current and projected practices that would be appropriate for inspecting nuclear reactors such as those in the background section of this thesis. The first nuclear reactors began operation in the 1940s and follow-on plants are successfully powering a substantial portion of the United States energy grid. There are multiple reactors currently in use and many more in the design phase. Because of this, it is appropriate to leverage previous approaches to conducting in-service inspections and test them against the parameters of the reactors of interest in this research. The methods most applicable to address ISI for LFRs include eddy-current testing, thermal, and acoustic methods.

The second part of this evaluation of ISI approaches, applies basic physics principles to the LFR to see if previous ISI techniques are compatible with the selected reactor properties. The LFR concepts chosen to provide a basis for evaluation of such techniques are the ELSY design and the Westinghouse Demonstration LFR, both previously identified in the background chapter. Below are the applicable reactor dimensions, properties, and physical parameters used in this research. The following is a discussion of the physics required to determine the degree of compatibility between the chosen inspection techniques and the reactor concepts under consideration.

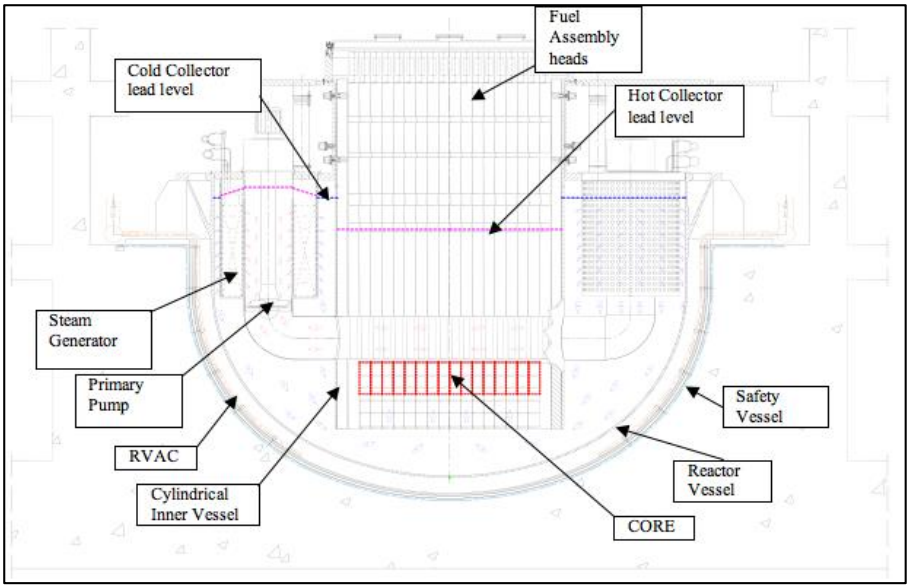

Figure 9. ELSY Sketch. Source: Smith and Cinotti (2016).

Table 6. Reactor testing parameters (ELSY). Source: Smith and Cinotti (2016).

Parameter	Measurement
Core Diameter	4.32 m
Core height	0.9 m
RV Diameter	11.5 m
Distance from RV to Core (bottom)	1.25 m
Distance from RV base to FLL	6.0 m
RV thickness	0.05 m
Core immersed in lead (below FLL)	4.75 m
Core inlet temp	400°C
Core outlet temp	480°C
Core maximum temp	550°C

Table 7. Reactor Materials (Westinghouse DLFR). Source: Westinghouse Electric Company, LLC. (2016).

Component	Material
Fuel	UO_2
Internal Assembly	D9 Stainless Steel (slight modification from AISI 316(L) Steel- will use 316 properties for study)
Coating for components >450^{0}C	AL_2O_3
Inner Vessel, Lower core plate, Main Vessel, SG Tubes	AISI 316(L) Steel

1. Eddy Current Testing

Eddy-current testing leverages Faraday's law of electromagnetic induction (below) to inspect for defects in conductive materials, where ε is the electromotive force and Φ_B is the magnetic flux density (García-Martín, Gómez-Gil, and Vázquez-Sánchez, 2011).

$$\varepsilon = \frac{d\Phi_B}{dt}$$

An eddy-current probe is a coil of wire with an alternating current which, using this principle induces an alternating magnetic field. That probe has a characteristic impedance, which is simply the voltage/current ratio. As the coil approaches a conductive surface, the surface produces its own circular currents (eddy-currents) which induce a secondary magnetic field, countering the probes magnetic field (García-Martín, Gómez-Gil, and Vázquez-Sánchez, 2011). This effect changes the impedance of the coil, which can be measured and used as the calibration for the ECT probe. When a crack or defect is approached in the same material, the impedance is increased (i.e., the magnetic field of the secondary field is distorted).

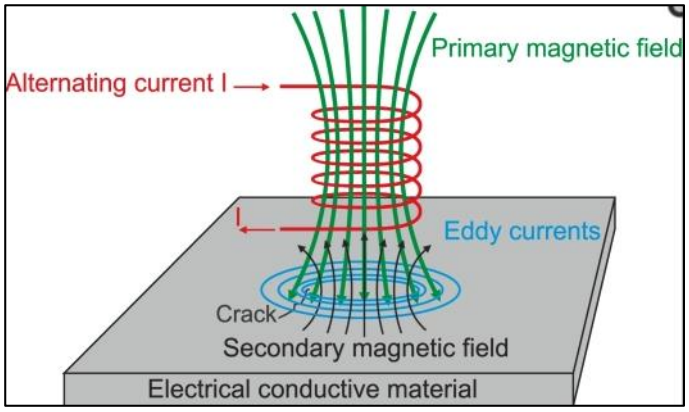

Figure 10. Sketch of ECT Physical Principles. Source: García-Martín, Gómez-Gil, and Vázquez-Sánchez (2011).

The main parameter to be considered for evaluation of reactor component materials is the penetration depth δ. It is calculated by:

$$\delta = \sqrt{\frac{2}{\mu\omega\sigma}}$$

where σ is the conductivity in 1/(Ωm), μ is the magnetic permeability $\mu = \mu_r\mu_0$ (both material properties), and ω is the angular frequency which is 2π times the frequency (García-Martín, Gómez-Gil, and Vázquez-Sánchez, 2011). This equation is based on the assumption of ~37% return signal (García-Martín, Gómez-Gil, and Vázquez-Sánchez, 2011), which is considered adequate in ECT. Although these individual parameters are important in ECT, their overall combination determines the maximum frequency used to inspect our entire component at a certain thickness.

2. Thermal

Thermal inspections are generally conducted through probing at certain areas and transmitting that signal through an electrical connection. This research considered primarily the thermal properties of materials where inspections are required. To test how temperature flows in a reactor, we considered the thermal diffusivity and the rate of convection. The thermal diffusivity, α is the rate of temperature diffusion of the medium in m^2/s. The thermal diffusivity is calculated from the thermal conductivity k, density, ρ, and specific heat at constant pressure, c_p, using:

$$\alpha = \frac{k}{\rho c_p}$$

The convection rate is given in the reactor specifications at 1.4 m/s in the Westinghouse Demonstration LFR shown in Table 3. Comparing the diffusivity to the lead flow caused by convection can give us a reasonable understanding of where to put thermal sensors.

3. Acoustic/Transduction

Because of the material properties of LFRs, many inspections may be conducted using acoustic means. This includes pressure transduction, ultrasound, and acoustic

probing. To test general design principles, all our simulations assume 1D geometry at normal incidence. This doesn't give exact answers, but does give an indication of whether or not the technology is compatible with our design.

According to Wilson (1988), "an electroacoustic transducer converts electrical energy to acoustical energy or vice versa." Acoustic transduction relies on the properties of sound in the medium and the medium's reaction when in contact with a transducer. A transducer can use piezoelectric materials that expand and contract when a voltage difference is applied. Additionally, piezoelectric materials give a voltage reading when expanded or contracted. For pressure transduction, as long as the wavelength of sound in the material is long compared to the dimensions of the transducer, the transducer will work in transduction (Wilson 1988, 107). When the pressure changes in a medium in contact with the transducer, it gives a voltage reading, calibrated to tell the pressure.

Ultrasound and acoustic probing use transducers as transmitters and receivers. For transmission, an alternating voltage is applied over the transducer at the frequency wanted. This voltage flexes the piezoelectric material, producing an oscillating pressure wave with wavelength inversely proportional to frequency. For receiving, the receiver expands and contracts straining the material. This strain variation in a piezoelectric gives a voltage reading, calibrated to give an image based on the return signal.

The signal travelling through a medium depends on several material properties. The acoustic impedance, r, is the density, ρ, times the speed of sound in the material, c, and determines how well sound transmits in a material. The acoustic absorption coefficient determines how much sound is absorbed in a material based on frequency and depth. It is dependent on several factors tabulated in Appendix A and gives the attenuation of sound in a given material in dB/m.

$$\alpha_c = 8.7 * \frac{\omega^2}{2\rho_o c^3}\left(\frac{4}{3}\eta + \frac{(\gamma-1)\kappa}{c_p}\right)$$

where ρ is the density, c_p is the specific heat at constant pressure, γ is the ratio of specific heats, κ is the thermal conductivity, η is the dynamic viscosity, and c is the speed of sound (Kinsler et al., 2000, 8.5.3). The coefficient, α_c, can also determine the amplitude

of the sound wave at a certain distance. For comparison, in water the absorption coefficient is shown in Figure 11.

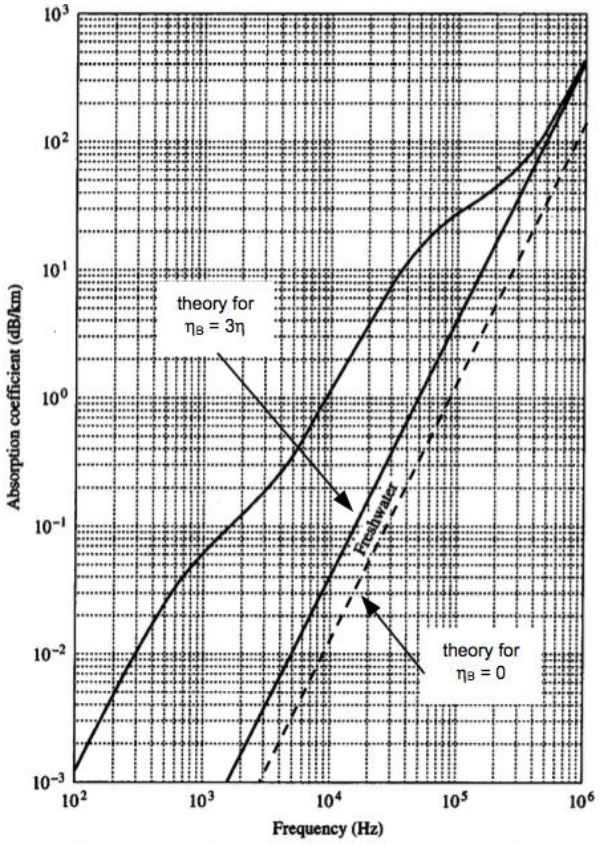

Figure 8.7.1 Sound absorption at $T = 5°C$ and $Z = 0$ km in freshwater and seawater (pH = 8, $S = 35$ ppt).

Figure 11. Sound Absorption Coefficient in Water by Frequency.
Source: Kinsler et al. (2000).

Because dBs are a logarithmic unit, a simple exponential can determine the amplitude of a sound wave after a certain distance, x:

$$A = A_0 * 10^{-\alpha_c x}.$$

where A and A_0 are the measured and initial amplitude.

To determine if we are in the far field for a cylindrical baffled source (where the signal can be approximated as a plane wave making calculations simpler), two conditions are shown on the following page. (Kinsler et al., 2000, 181)

$$d \gg a \; and \; d \gg \frac{a^2}{\lambda}$$

where d is the distance traveled, a is the radius of the source, and λ is the wavelength.

Finally, to determine how much signal is reflected between two different media, we need to determine the intensity transmission and reflection coefficients, which are (Kinsler et al., 2000, 151-152)

$$R_I = \left(\frac{r_2 - r_1}{r_2 + r_1}\right)^2 \text{ and } T_I = 1 - R_I$$

where R_I is the power reflection coefficient, T_I is the intensity transmission coefficient (both as a percentage of intensity), and r is the specific acoustic impedance of each material.

The combination of these variables should give us a good idea of how much signal we'll receive through acoustic measurements, and how clear that signal will be.

THIS PAGE INTENTIONALLY LEFT BLANK

IV. RESULTS

To begin the discussion of results, all applicable parameters were calculated at the lower and higher expected temperatures of lead within the reactor. The equations used to calculate these values were taken from Vitaly and Sobolev's 2010 article, "Database of Thermophysical Properties of Liquid Metal Coolants for GEN-IV." The equations used are shown in Appendix A, and the MATLAB code used to process these equations at the appropriate temperatures is shown in Appendix B. For comparison, sodium at an operating temperature of 550 ^{0}C for an SFR is calculated.

Table 8. Values Required in Lead and Sodium for Testing ISI Parameters (Calculated in Appendix B).

Parameter	**Lead at 400^{0}C**	**Lead at 480^{0}C**	**Sodium at 550^{0}C**
Density [kg/m^3]	10600	10500	832
Speed of sound [m/s]	1790	1770	2310
Impedance [kg/m^{2}s]	1.90 e7	1.86 e7	0.192 e7
Specific heat constant pressure [J/kg*K]	146	145	1260
Specific heat constant volume [J/kg*K]	123	120	1000
Isobaric thermal expansion coefficient [K^{-1}]	1.21 e-4	1.22 e-4	2.82 e-4
Isentropic bulk modulus [Pa]	2.99 e10	2.90 e10	4.46 e9
Isothermal bulk modulus [Pa]	2.51 e10	2.39 e10	3.53 e9
Thermal conductivity [W/m*K]	16.6	17.5	67.7
Dynamic Viscosity [Pa*s]	2.23 e-3	1.88 e-3	2.36 e-4

Additionally, the material properties required for testing our stainless steel and aluminum oxide coating are shown on the following page. Because the speed of sound wasn't specified in the design parameters, we used the base equation:

$$c = \sqrt{\frac{B_s}{\rho}}$$

where B_s is the bulk modulus of the material.

Table 9. Values Required in AISI 316(L) and Al_2O_3 for Testing ISI Parameters.

Parameter	D9/AISI 316(L)	Al_2O_3
Density [kg/m^3]	7990	3980
Speed of sound [m/s]	4360	7670
Impedance [kg/m^{2}s]	3.48 e7	3.05 e7
Maximum use Temp [°C]	1700	1198
Magnetic Permeability	1.28e-6	-
Electrical Resistivity [μΩ-cm]	74	-
Electrical Conductivity [1/Ωm]	1.35 e6	-

Source: AZO Materials n.d. and Accuratas (2013).

A. LEAD COOLANT MONITORING

From our methodology, the coolant requires inspections of the temperature ensure proper heat removal from the core, coolant flow, and the temperature staying above the freezing point of lead. Inspection of the coolant composition and free lead level require no additional comparison as they can be accomplished with current technology as discussed in our background.

1. Adaptation from Previous Design/Technology

Of our two discussed temperature sensors, thermocouples can handle a chaotic environment at higher temperatures. Therefore, they are a better fit for LFRs. According to an article in *Power Engineering Magazine*, thermocouples used in nuclear reactors are accurate up to 3100 ^{0}C but dependent on direct wiring from the thermocouple to the monitoring device (Jethra, 2013). Three currently used thermocouples are as follows:

- For temperatures < 1,000 °F and mounting locations subject to vibration, as well as low-corrosion atmospheres: NiCr-Ni (Type K)
- For temperatures < 1,832 °F and corrosive atmospheres: NiCr-Ni (Type N)
- For temperatures > 1,832 °F: Pt Rh-Pt (Types R and S).

Type K thermocouples are good under 1000°F which only translates to about 530°C. Because we have estimated core temperatures of 550°C and need temperature sensing above that, it cannot be used. The second thermocouple type has a temperature

range (up to 1832F or 1000C) that encompasses the operational range of an LFR and would be applicable to such a reactor system. The third type is intended for much higher temperatures than would be encountered in an LFR. The internal properties of the thermocouple are dependent more on temperature than outside environment. In the heavily corrosive environment of molten lead, using a Type N thermocouple plated with Al_2O_3 could provide the corrosion resistance required, at a temperature resistance far exceeding reactor parameters.

2. Physics Applied

The main concern for temperature measurement in a lead cooled fast reactor is coolant flow and ensuring that steady state conditions exist in the reactor. The question becomes where to put the temperature sensor to get an accurate picture. Calculating the diffusivity of temperature in lead at the high and low end is carried out as follows:

$$\alpha_{480°C} = \frac{\lambda}{\rho c_p} = \frac{17.5}{10500 * 145} * \frac{10^6 mm^2}{1 m^2} = 11.5 \frac{mm^2}{s}$$

$$\alpha_{400°C} = \frac{\lambda}{\rho c_p} = \frac{16.6}{10600 * 146} * \frac{10^6 mm^2}{1 m^2} = 10.7 \frac{mm^2}{s}$$

The lead flow rate is 1.4 m/s. To do a comparison between these two levels of diffusivity, you can consider the situation where a 1mm by ~11mm column of lead is heated every second by a core element. Within that second, the coolant column travels 1400mm away. In steady state, the convection caused by heating heavily dominates the diffusion throughout the reactor in directions other that of the lead flow.

Placing thermocouples in the natural path of lead flow distributed across the reactor will give you a clear picture of the temperature distribution. If lead is moving out of the normal flow path, the temperature will show out of steady state conditions in the affected area. This will give an accurate temperature picture of the inside of an LFR.

B. REACTOR INTERNAL COMPONENTS

The core and internal components require temperature sensing and an overall idea of the integrity of core components. Thermal measurements of the core and internal components can use the same inspection devices as the coolant. Because convection far outpaces diffusion in thermal transport, placing thermocouples ahead of critical components in the direction of lead flow can generate a clear overall picture of individual component temperatures. The internal component integrity, however, must be imaged or inspected in some way.

1. Adaptation from Previous Design/Technology

Previous designs for inspecting the integrity of core components involved removal of core components on a periodic cycle for physical inspections. This is one of the main reasons for the pool type reactor design in LFRs. As discussed previously, SFR research has determined ultrasonic transduction is attainable for internal component inspection. Further development of material science is required to determine what material is required on the surface of the transducer to achieve coupling between the transducer and molten lead with, in addition, material compatibility to avoid the effects of lead corrosion.

2. Physics Applied

Three acoustic variables must be determined to see if ultrasonic transduction is attainable in a LFR. First, the attenuation of sound is determined to see how far our signal will reach under different circumstances in lead. This is compared to sodium and water for reference. Second, the maximum size transducer is calculated by our core dimensions, ensuring our ultrasonic signal remains in the far field. Finally, the transmission and reflection intensity coefficients are determined to see how much signal is returned when reaching the coolant-component boundaries.

Using our theory and values from Appendix A, the attenuation of sound in molten lead is graphed, varying the frequency in ultrasonic range, between 50 kHz and 10MHz.

Substituting the required variables and calculating in MATLAB (Appendix B), the following graph is produced:

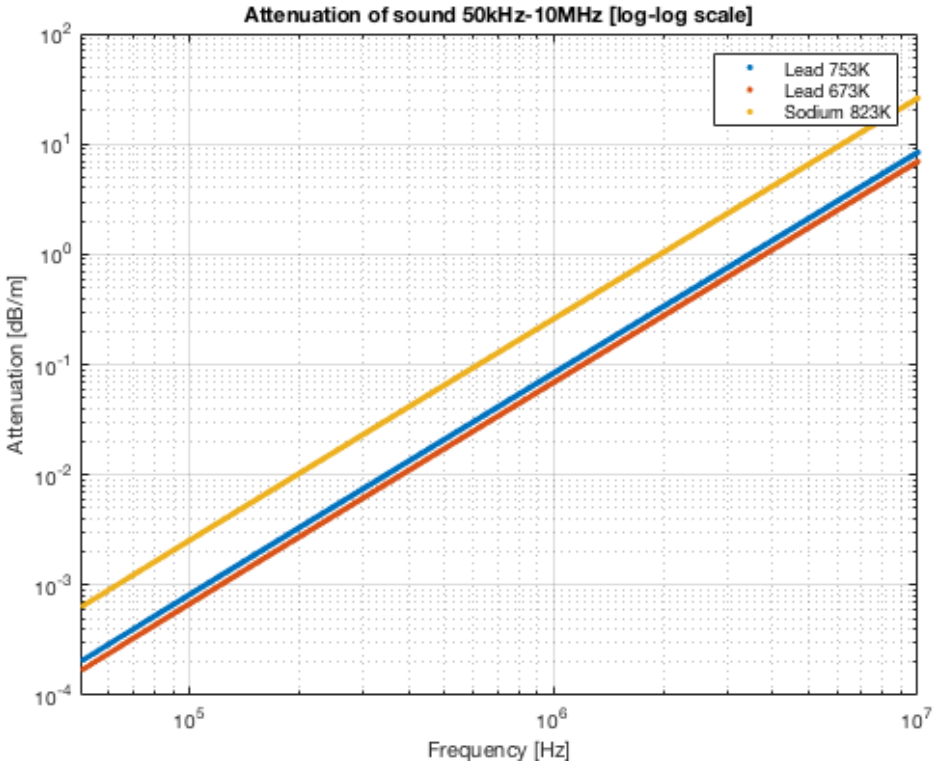

Figure 12. Sound Attenuation of Sodium and Lead (Code in Appendix B).

This shows that under all conditions, the attenuation of sound in lead is less than in sodium. Additionally, comparing lead, sodium, and freshwater at 1MHz, the attenuation in freshwater is ~ .4dB/m (400dB/km from Figure 11), the attenuation in sodium is ~.2dB/m, and the attenuation in lead at the higher temperature is ~.05dB/m. Therefore, this reduced attenuation should have no effect on resolution in ultrasonic imaging.

To get a clear understanding of signal losses in molten lead, the relative intensity of the initial signal can be measured against the distance the signal travels an exponential.

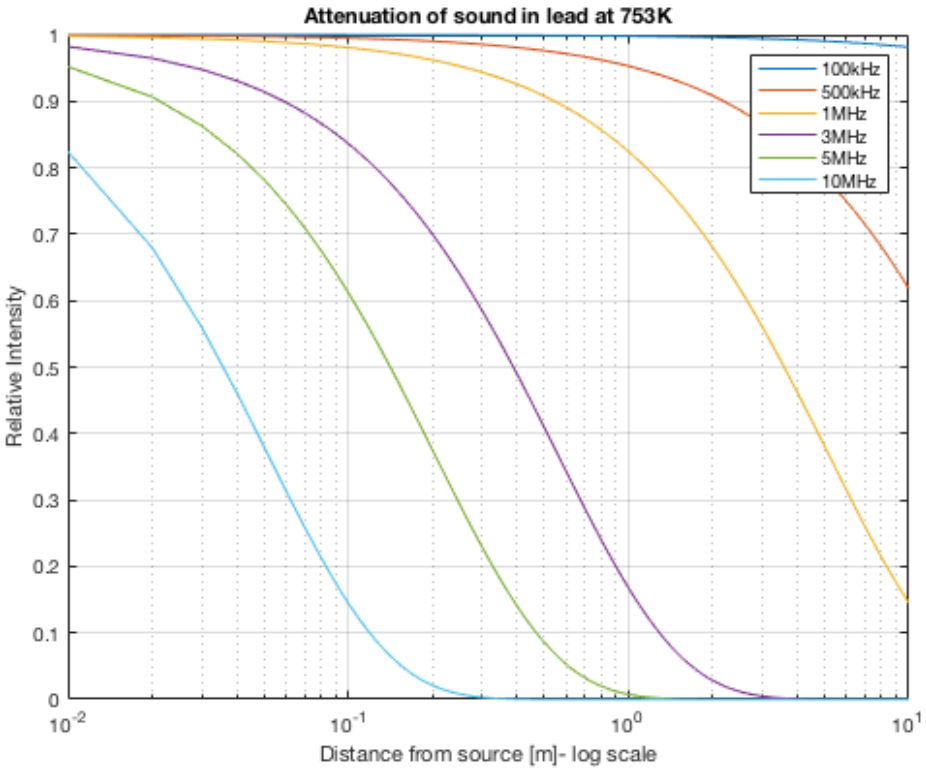

Figure 13. Sound Loss by Distance at Different Frequencies in Lead (Code in Appendix C).

Using a variety of frequencies at the maximum temperature (maximum signal loss in the reactor), the approximate distance to signal loss can be seen. Therefore, if the transducer assembly is located at the bottom of the reactor vessel, to obtain a picture of the bottom of the core at 1.5m (3.0m round trip), the signal must be below 3MHz. To obtain a picture of the top of the core at 6.0m (12m round trip), the signal must be below 1MHz.

The second test for ultrasonic transduction is the maximum radius of the transducer to ensure meeting the far field condition. To recount, the two conditions that are required to be met are $d \gg a$ and $d \gg \frac{a^2}{\lambda}$, where d is the distance between the transducer and the assembly, a is the radius of the transducer, and λ is the wavelength. For this study, we used an order of magnitude as "much greater than" to ensure we are in the far field. Therefore, the first condition is met as long as the transducer radius is less than 15cm, which is reasonable. The second condition is wavelength dependent. Because

the attenuation restricts our frequency to lower than 10MHz, the range specified is between 1MHz and 5MHz. When compared to frequency, our second condition becomes $d \gg \frac{a^2 f}{c}$. Setting the right side equal to 15cm to ensure the far field condition and using the speed of sound in lead at our outlet temperature of 1770m/s, our maximum radius of the transducer can be between .73cm (5MHz) and 1.6cm (1MHz). The transducer used in sodium testing was ½" diameter, which is .64cm radius. The radius range calculated is attainable and reasonable for the frequencies expected.

The final test is the reflection of a signal when interacting with components. Using the equations for reflection and transmission intensity, the specifications for lead at 480°C, the assumption of 1.5m between the transducer and the components, and a 1mm thick Al_2O_3 coating, the reflection and transmission coefficients are listed in Table 10. For comparison, the sodium-316(L) SS reflection is noted.

Table 10. Reflection and Transmission at Component Boundaries (Code in Appendix D).

Boundary	Reflection	Transmission
Lead- Al_2O_3	5.9%	94.1%
Al_2O_3- 316(L) SS	0.4%	99.6%
Sodium- 316(L) SS	80.2%	19.8%

The transmission and reflection is highly dependent on the impedance mismatch between the coolant and the component. The impedance of sodium and water are 1.96 e6 and 1.5 e6 kg/m^{2}s, showing similarity. The impedance of lead is an order of magnitude higher at 1.9 e7 kg/m^{2}s, which is closer to the component impedance of 3.05 e7 kg/m^{2}s. This gives a greater transmission of signal through the coolant-component boundary than a pressure wave in water or sodium. Additionally, the near acoustic match between the coating and the component material ensures there is little to no internal reflection once the signal is transmitted in the component.

The low reflection in lead compared to sodium puts initial doubt in the possibility of acoustic diagnostics in an LFR. However, when combining the percentage of reflection

with the attenuation of sound in the medium, a clearer picture is shown for the relative intensity of input vs. received signal. The graph is shown at 1MHz, but because the attenuation relationship is linear between sodium and lead, similar results would occur regardless of frequency.

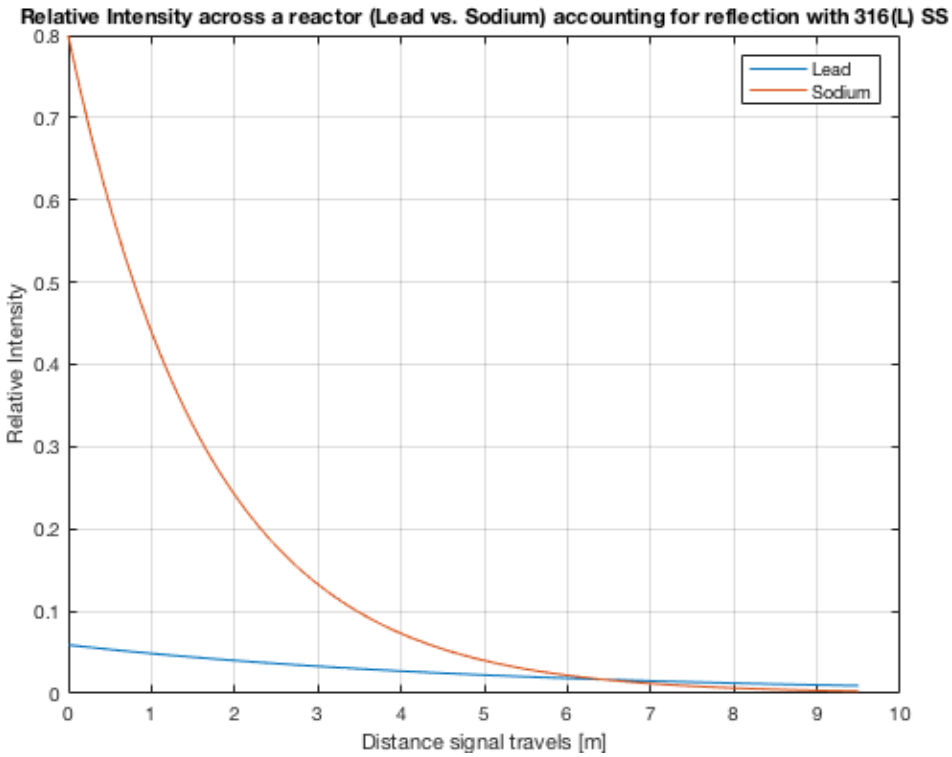

Figure 14. Intensity Loss by Distance of Lead versus Sodium Accounting for Reflection (Code in Appendix G).

It is shown, above a distance from the transducer of ~3.25m (6.5m total sound travel distance), lead is superior to favorable acoustically to sodium at 1MHz. Although there is little reflection, the returned signal in lead is comparable and eventually better than sodium at a farther probing distance.

C. REACTOR VESSEL

The reactor vessel is 50mm of AISI 316(L) stainless steel as outlined in our background. There is an air gap between the containment structure and the RV for

inspection purposes (Westinghouse Electric Company, LLC., 2016). The main inspections required involve integrity of the RV and corrosion detection.

1. Adaptation from Previous Design/Technology

Previous nuclear reactor designs used inspection tools inside of the reactor vessel to minimize exposure of personnel and take advantage of visual inspections. The RPV-ISI Tool uses visual, electrical, and acoustic inspection methods to assess corrosion and integrity of the RPV to a depth of 40mm (Pajnić et al., 2010). The opaque properties of lead rule out visual inspections of the LFR's reactor vessel from the inside. Because of the corrosive nature of lead, the air gap between the reactor vessel and the outside containment is used to house inspection tools.

2. Physics Applied

For eddy-current testing (ECT), the skin depth of penetration is applied to determine if it is feasible to conduct such testing from the outside of the reactor. Typical ECT frequencies occur between 100Hz and 25MHz (García-Martín, Gómez-Gil, and Vázquez-Sánchez, 2011). We can test the penetration depth from 1mm to 50mm to test the full frequency range required.

$$\delta = \sqrt{\frac{2}{\mu\omega\sigma}} \rightarrow f = \frac{1}{\pi\mu\sigma\delta^2}$$

For a 1mm penetration depth, a frequency of 184kHz is required which is attainable and in our frequency range. At a 50mm depth, the frequency lowers to 74Hz, which is outside the range for a typical ECT. Using the original equation, at 100Hz the maximum penetration depth increases to 42.9mm. This is the maximum depth of penetration for an ECT using current technology. For the RV current thickness of 50mm, it is unattainable to detect flaws at the surface of the inner vessel from the outside.

Short range ultrasonic testing is less dependent on the signal reaching the far field since the transducer is coupled with the tested material. Because of this, the attenuation of sound in steel and the reflection at the lead boundary are the primary concerns. After thorough research, the conclusion is that there is no current data on absorption of sound

in AISI 316 (L) Stainless steel. The acoustic properties of AISI are similar though to general steel. In "Acoustic Emissions in Geotechnical Engineering Practice" (Korner, McCabe, and Lord, 1981), there is an estimate of the attenuation coefficient by frequency for steel as was previously described for lead. Although not exact, it gives a general idea of how sound reacts in the reactor vessel.

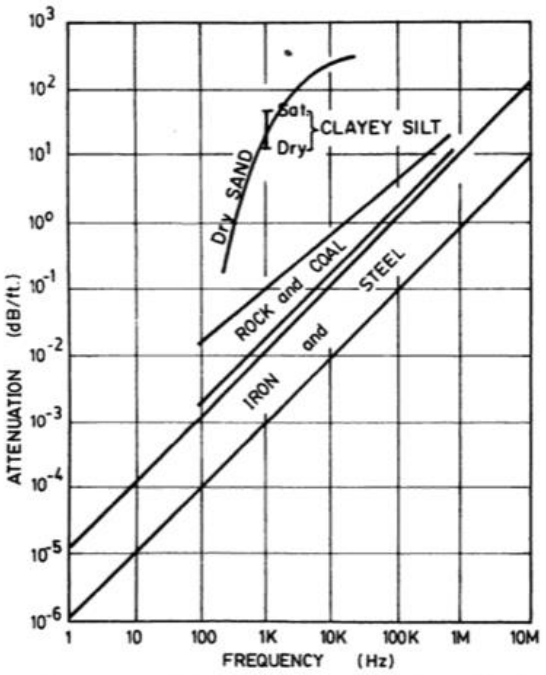

FIG. 5—*Attenuation response of different soil types contrasted to rock/coal and iron/steel.*

Figure 15. Sound Attenuation in Steel. Source: Korner, McCabe, and Lord (1981).

Once again, ultrasound typically uses frequencies from 50kHz to 10MHz. Taking several data points from Figure 15, the attenuation of steel for a typical range of frequencies can be plotted to give a general idea of frequency range required for use in transduction for Non-Destructive Testing.

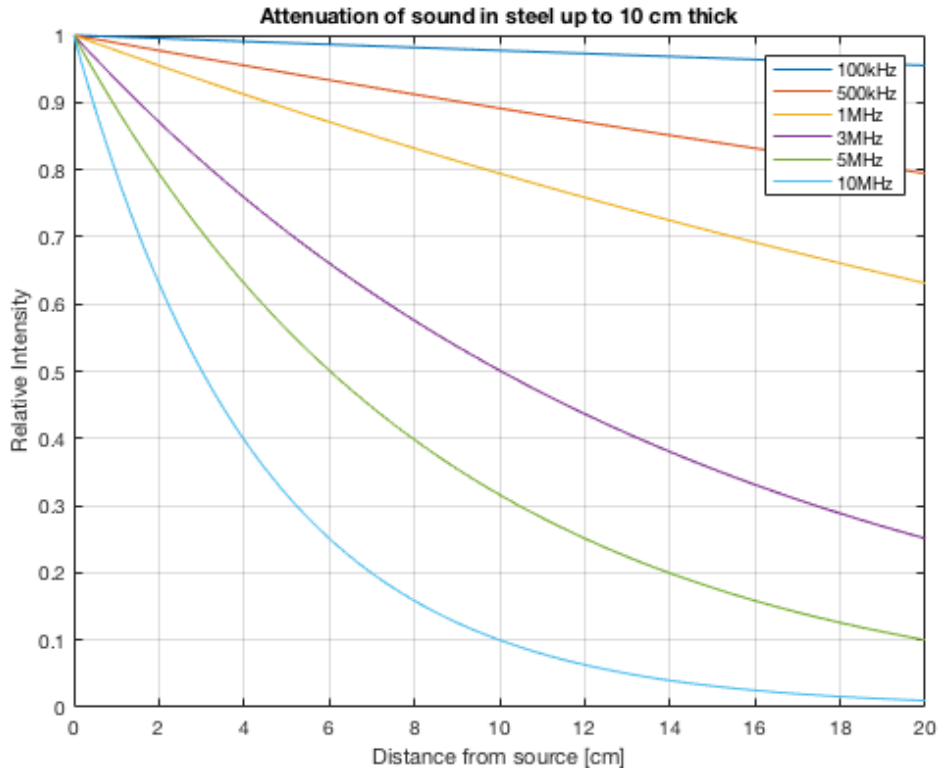

Figure 16. Intensity Loss by Distance at Different Frequencies in AISI 316 (L) (Code in Appendix F).

For reactor vessels, up to 10cm thick (20cm traveling distance), a relative intensity of greater than 20% is received after the reflection of signal with a frequency of less than 5MHz. This meets all current designs for LFR reactor vessels.

The next test is checking reflection at the boundary of the reactor vessel and the coolant. The reflection coefficient between steel and lead is:

$$R_I = \left(\frac{r_2 - r_1}{r_2 + r_1}\right)^2 = \left(\frac{(1.86 - 3.48) * 10^7}{(1.86 + 3.48) * 10^7}\right)^2 * 100 = 5.4\%$$

Although this is small, the RV-coolant boundary is not what the transducer is trying to detect. With a noticeable difference in material density due to corrosion, or a change of impedance due to a crack, the reflection will increase. This increase is calibrated to return a response and give the inspector an idea of the deformation.

Ultrasonic inspection shows compatibility with short range inspections for the reactor vessel. It is, however, not practical to encompass the entire RV with transducers. This would cause more acoustic noise in the RV, and potentially cause instability in the coolant. Therefore, a periodic inspection is more reasonable. Additionally, higher frequency can give better resolution for ultrasonic inspections. Therefore, it may still be favorable to conduct this inspection from inside the RV to get a better indication of surface conditions.

D. STEAM GENERATORS

The steam generators are inspected for corrosion and defects. In general, the geometry and materials of the steam generators can change, but the methods for conducting inspections remain the same. Steam generators cycle the coolant through a pumping system next to a pressurized flowing steam channel. Previous approaches include inspections in the steam generator that are conducted periodically through ECT, sending a probe through the SG tubes.

1. Adaptation from Previous Design/Technology

The steam generator tubes in the selected data for a representative LFR are 4–5 mm thick and made of AISI 316 (L) Stainless Steel. The main issue to address is the compatibly of ECT with AISI 316 (L) Steel.

2. Physics Applied

The result of an initial physics evaluation found that ECT was not compatible with RV surface inspections. However, the general equation for testing penetration depth of ECT can be applied to check for thick SG tubing. Rearranging the penetration depth equation, we can test depth as a function of frequency:

$$\delta = \sqrt{\frac{1}{\mu\sigma\pi f}}$$

Varying the frequency within the acceptable range of 100Hz to 20MHz and plotting against penetration depth produces a graph of acceptable frequencies and their maximum penetration depth shown below.

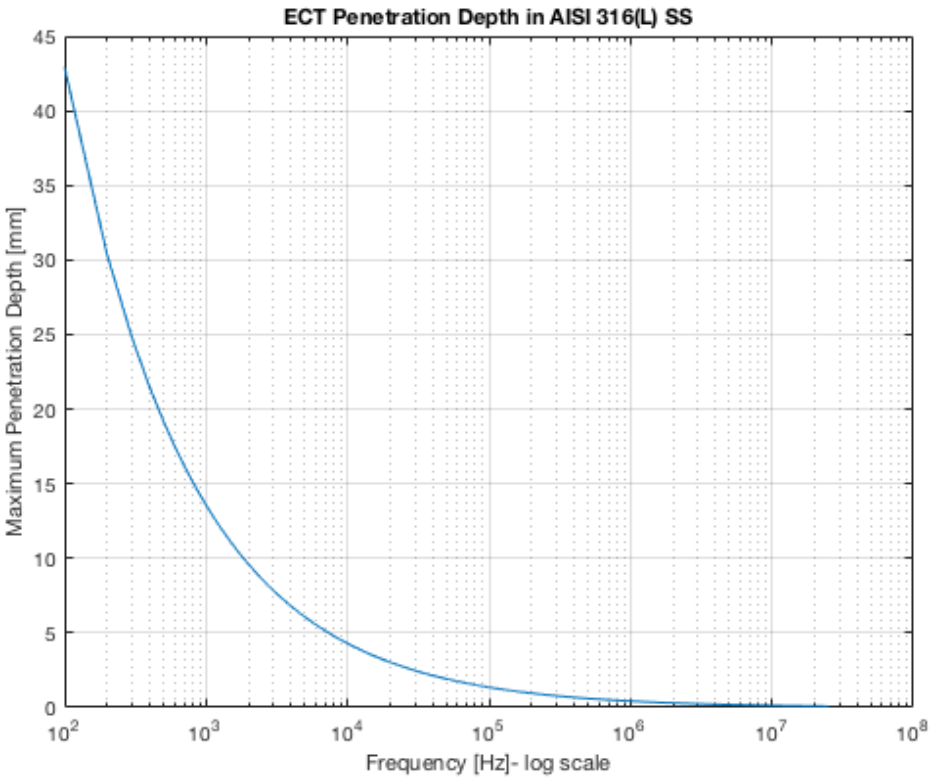

Figure 17. ECT Penetration Depth at Available Frequencies (Code in Appendix E).

At 5mm, a frequency of ~7,000 Hz or less can penetrate and test the SG tubes. As the thickness of the SG tube decreases, the maximum frequency increases exponentially. This is within our design parameters for ECT systems, which vary between 100Hz and 25MHz (García-Martín, Gómez-Gil, and Vázquez-Sánchez, 2011).

THIS PAGE INTENTIONALLY LEFT BLANK

V. SUMMARY, CONCLUSIONS, AND RECOMMENDATIONS

In summary, this thesis identified requirements for ISI based on NRC design criteria and the general layout of an LFR. Of those requirements, six inspections were considered unique to the LFR and requiring further development. There is current technology available that is compatible with each inspection, as shown in in Table 11. The inspections, recommended methods, and frequency of inspection are listed below.

Table 11. Summary of Scientific Study.

Component	Inspection	Method	Frequency
Coolant	Temperature	Type N thermocouples Al_2O_3 coated distributed throughout core	Continuous
Coolant	Filtration	Remove and test ceramic filters in SG	Periodic- during scheduled services
Core	Components	Ultrasonic transduction from base of RV	Continuous
Core	Temperature	Type N Thermocouples Al_2O_3 coated distributed ahead of critical components in lead flow path	Continuous
RV	Integrity	Ultrasonic transduction from air gap between RV and main vessel	Continuous-scanning
SG	Integrity	Eddy current testing through probing in SG tubes	Periodic- during scheduled services

Of these, the temperature measurements, filtration, and SG inspections can be conducted with tested technology. As LFRs develop, these technologies are commercially available for testing and implementation. The core components and reactor vessel inspections by ultrasound require more development. There is little reflection at the boundaries, due to the acoustic similarity between lead, AL_2O_3, and AISI 316(L) SS. Because of the low attenuation of sound at higher frequencies in lead, it is still comparable to current technology developed for use in SFRs at typical reactor dimensions. Therefore, ultrasonic inspections are feasible with current physics theory applied, but testing is not complete to ensure a distinguishable signal.

Many current LFR designs have all components removable for periodic inspections. Technology dictates steam generators are required to be shut down to conduct ECT and coolant filtration inspections. If inspectors alternate which SG is offline during an outage, inspectors can conduct these inspections on SGs one at a time while maintaining reactor function. However, if the reactor is required to be shut down, it would be wise to follow current practices of inspection by component removal. A combination of ultrasound to get a general core image, temperature to monitor coolant parameters, and periodic filter inspection to detect corrosion in materials can give a good indication of malfunctions in the core. Individually, though, ultrasound remains untested in similar conditions.

A. RECOMMENDATIONS FOR FUTURE RESEARCH

Although currently used technology makes ISI possible to meet NRC design criteria, further testing is required to ensure an adequate picture of the core and reactor vessel is achievable. For modeling research, 3D multi-physics simulations can give a better understanding of the transmitted acoustic signal of an LFR under operating conditions. They can also give an indication of the temperature distribution and coolant flow pattern based on this distribution.

For physical research, lead at operating LFR temperature has almost identical acoustic impedance to liquid mercury at room temperature (Kinsler et al., 2000, 527). Therefore, short range testing in mercury may give a better indication of the compatibility of ultrasonic transduction when used inspecting LFRs. It eliminates the need to test materials in a hot corrosive environment to determine their acoustic capabilities.

Finally, for policy research, the economic and military implications of using an LFR in a microgrid are of interest. This includes economic return of LFRs within the United States energy grid, and further research of the feasibility using an LFR in a deployable setting. Comparisons can be made to current microgrid structures in the United States and ways the LFR counters nuclear proliferation.

APPENDIX A. EQUATIONS FOR MOLTEN LEAD PARAMETERS

The equations were taken from Sobolev (2010) and used in determining our parameters for molten lead.

Density: $\rho = 11441 - 1.2796\ x\ T$
Specific heat constant pressure: $c_p = 176.2 - 4.923\text{e}^{-2} * \text{T} + 1.544\text{e}^{-5}\ \text{x}\ \text{T}^2 - 1.524\text{e}^{6}\ \text{x}\ \text{T}^2$
Isobaric volumetric thermal expansion coefficient: $\alpha_p = \frac{1}{8942 - T}$
Isentropic bulk modulus: $B_s = (38.02 - 1.296\text{e}^{-2}\ \text{x}\ \text{T} + 1.32\text{e}^{-6}\ \text{x}\ \text{T}^2)e^9$
Isothermal bulk modulus: $B_t = \left(\frac{1}{B_s} + \frac{T\ \alpha_p^2}{\rho\ c_p}\right)^{-1}$
Specific heat constant volume: $c_v = c_p - \frac{\alpha_p^2\ \text{B}_t\ \text{T}}{\rho}$
Ratio of specific heats $\gamma = \frac{c_p}{c_v}$
Thermal conductivity: $\kappa = 9.2 + .011\ x\ T$
Dynamic Viscosity: $\eta = 4.55\ x\ 10^{-4} \exp\left(\frac{1069}{T}\right)$
Speed of sound: $c = 1953 - .246\ x\ T$

THIS PAGE INTENTIONALLY LEFT BLANK

APPENDIX B. ABSORPTION COEFFICIENT MATLAB CODE

```
%Find attenuation in different materials
clear
clc
%Input
%1= lead, 2=sodium 3= lead lower
T1= 753;%input('Input Upper Temperature for Lead in Kelvin: '); %temperature in
K
T3= 673;%input('Input Lower Temperature for Lead in Kelvin: '); %temperature in
K
T2= 823;%input('Input Temperature for Sodium in Kelvin: '); %temperature in K

%initialize values based on temperature
rho1=11441-1.2796*T1; %density
rho3=11441-1.2796*T3;
rho2=1014-0.235*T2;

cp1=176.2-((4.923e-2)*T1)+((1.544e-5)*T1^2)-((1.524e6)*T1^-2);  %Specific  heat
constant pressure
cp3=176.2-((4.923e-2)*T3)+((1.544e-5)*T3^2)-((1.524e6)*T3^-2);
cp2=(-3.001e6*T2^-2)+1658-0.8479*T2+(4.454e-4*T2^2);

ap1=1/(8942-T1);%isobaric volumetric thermal expansion coefficient
ap3=1/(8942-T3);
ap2=1/(4316-T2);

Bs1=(38.02-1.296e-2*T1+1.32e-6*T1^2)*(10^9); %isentropic bulk modulus
Bs3=(38.02-1.296e-2*T3+1.32e-6*T3^2)*(10^9);
Bs2=(7.542-4.634e-3*T2+8.326e-7*T2^2)*(10^9);

Bt1=((1/Bs1)+((T1*ap1^2)/(rho1*cp1)))^-1; %isothermal bulk modulus
Bt3=((1/Bs3)+((T3*ap1^2)/(rho3*cp3)))^-1;
Bt2=((1/Bs2)+((T2*ap2^2)/(rho2*cp2)))^-1;

cv1= cp1-((ap1^2*Bt1*T1)/rho1); %specific heat constant volume
cv3= cp3-((ap3^2*Bt3*T3)/rho3);
cv2= cp2-((ap2^2*Bt2*T2)/rho2);

gamma1=cp1/cv1; %ratio specific heats
gamma3=cp3/cv3;
gamma2=cp2/cv2;

kappa1=9.2+.011*T1; %thermal conductivity medium pg 147
kappa3=9.2+.011*T3;
kappa2=104-0.047*T2;
```

```
n1=4.55e-4*exp(1069/T1); %dynamic viscosity
n3=4.55e-4*exp(1069/T3);
n2=exp((556.835/T2)-(.3958*log(T2))-6.4406);

c1=1953-.246*T1; %sound speed
c3=1953-.246*T3;
c2=2723-0.531*T2;

f(1)=50000;
a1(1)=0;
a2(1)=0;
it=1;

while f(it) <= 10000000, %specify frequency upper limit
  a1(it+1)=(8.7)*(((2*3.14156*f(it))^2/(2*rho1*c1^3))*((4*n1/3)+((gamma1-
1)*kappa1/cp1))); %absorption coefficient
  a3(it+1)=(8.7)*(((2*3.14156*f(it))^2/(2*rho3*c3^3))*((4*n3/3)+((gamma3-
1)*kappa3/cp3)));
  a2(it+1)=(8.7)*(((2*3.14156*f(it))^2/(2*rho2*c2^3))*((4*n2/3)+((gamma2-
1)*kappa2/cp2)));
  f(it+1)=f(it)+1000;
  it=it+1;
end
  loglog(f,a1,'.')
  hold all
  loglog(f,a3,'.')
  loglog(f,a2,'.')
  axis([50000 10000000 10^-4 10^2])
  grid on
  title('Attenuation of sound 50kHz-10MHz [log-log scale]')
  xlabel('Frequency [Hz]')
  ylabel('Attenuation [dB/m]')
  legend('Lead 753K','Lead 673K','Sodium 823K')

fprintf('Lead at %g',T1);
fprintf('Pb Density[kg/m^3]: %g\n',rho1);
fprintf('Pb Sound speed[m/s]: %g\n',c1);
fprintf('Pb Specific heat constat pressure[J/kg*K]: %g\n',cp1);
fprintf('Pb Specific heat constat volume[J/kg*K]: %g\n',cv1);
fprintf('Pb Isobaric thermal expansion coefficient[1/K]: %g\n',ap1);
fprintf('Pb Isentropic bulk modulus[Pa]: %g\n',Bs1);
fprintf('Pb Isothermal bulk modulus[Pa]: %g\n',Bt1);
fprintf('Pb Thermal conductivity of lead[W/m*K]: %g\n',kappa1);
fprintf('Pb Dynamic viscosity[Pa*s]: %g\n',n1);

fprintf('Lead at %g',T3);
fprintf('Pb Density[kg/m^3]: %g\n',rho1);
fprintf('Pb Sound speed[m/s]: %g\n',c1);
fprintf('Pb Specific heat constat pressure[J/kg*K]: %g\n',cp1);
```

```
fprintf('Pb Specific heat constat volume[J/kg*K]: %g\n',cv1);
fprintf('Pb Isobaric thermal expansion coefficient[1/K]: %g\n',ap1);
fprintf('Pb Isentropic bulk modulus[Pa]: %g\n',Bs1);
fprintf('Pb Isothermal bulk modulus[Pa]: %g\n',Bt1);
fprintf('Pb Thermal conductivity of lead[W/m*K]: %g\n',kappa1);
fprintf('Pb Dynamic viscosity[Pa*s]: %g\n',n1);

fprintf('Na Density[kg/m^3]: %g\n',rho2);
fprintf('Na Sound speed[m/s]: %g\n',c2);
fprintf('Na Specific heat constat pressure[J/kg*K]: %g\n',cp2);
fprintf('Na Specific heat constat volume[J/kg*K]: %g\n',cv2);
fprintf('Na Isobaric thermal expansion coefficient[1/K]: %g\n',ap2);
fprintf('Na Isentropic bulk modulus[Pa]: %g\n',Bs2);
fprintf('Na Isothermal bulk modulus[Pa]: %g\n',Bt2);
fprintf('Na Thermal conductivity of lead[W/m*K]: %g\n',kappa2);
fprintf('Na Dynamic viscosity[Pa*s]: %g\n',n2);
```

```
Lead at 753

Pb Density[kg/m^3]: 10477.5

Pb Sound speed[m/s]: 1767.76

Pb Specific heat constat pressure[J/kg*K]: 145.197

Pb Specific heat constat volume[J/kg*K]: 119.59

Pb Isobaric thermal expansion coefficient[1/K]: 0.000122115

Pb Isentropic bulk modulus[Pa]: 2.90096e+10

Pb Isothermal bulk modulus[Pa]: 2.38935e+10

Pb Thermal conductivity of lead[W/m*K]: 17.483

Pb Dynamic viscosity[Pa*s]: 0.00188174

Lead at 673Pb

Density[kg/m^3]: 10477.5

Pb Sound speed[m/s]: 1767.76

Pb Specific heat constat pressure[J/kg*K]: 145.197

Pb Specific heat constat volume[J/kg*K]: 119.59

Pb Isobaric thermal expansion coefficient[1/K]: 0.000122115

Pb Isentropic bulk modulus[Pa]: 2.90096e+10
```

```
Pb Isothermal bulk modulus[Pa]: 2.38935e+10

Pb Thermal conductivity of lead[W/m*K]: 17.483

Pb Dynamic viscosity[Pa*s]: 0.00188174

Na Density[kg/m^3]: 820.595

Na Sound speed[m/s]: 2285.99

Na Specific heat constat pressure[J/kg*K]: 1257.43

Na Specific heat constat volume[J/kg*K]: 981.918

Na Isobaric thermal expansion coefficient[1/K]: 0.000286287

Na Isentropic bulk modulus[Pa]: 4.29216e+09

Na Isothermal bulk modulus[Pa]: 3.35172e+09

Na Thermal conductivity of lead[W/m*K]: 65.319

Na Dynamic viscosity[Pa*s]: 0.000220195
```

Published with MATLAB® R2016a

APPENDIX C. ATTENUATION IN LEAD MATLAB CODE

```
%Attenuation of sound in lead at 753K
clear
clc
x=0:.01:10;
A2=10.^(-x.*(8.12e-4)); %100kHz
A3=10.^(-x.*(.0209)); %500kHz
A4=10.^(-x.*(.0838)); %1MHz
A5=10.^(-x.*(.775)); %3MHz
A6=10.^(-x.*(2.13)); %5MHz
A7=10.^(-x.*(8.39)); %10MHz
semilogx(x,A2)
hold all
semilogx(x,A3)
semilogx(x,A4)
semilogx(x,A5)
semilogx(x,A6)
semilogx(x,A7)
grid on
title('Attenuation of sound in lead at 753K')
xlabel('Distance from source [m]')
ylabel('Relative Intensity')
legend('100kHz','500kHz','1MHz','3MHz','5MHz','10MHz')
```

Published with MATLAB® R2016a

THIS PAGE INTENTIONALLY LEFT BLANK

APPENDIX D. REFLECTION/TRANSMISSION OF COMPONENTS IN LEAD MATLAB CODE

```
% 1D reflection transmission problem for reactor component materials
% at normal incidence, Lead at 400C
clear
clc
%Initialize impedance (r)
% 1- lead at 480C, 2- Al2O3, 3- AISI 316L SS 4- Sodium
rho1=10500;c1=1770; r1=rho1*c1;
rho2=3980;c2=7670; r2=rho2*c2;
rho3=7990;c3=4360; r3=rho3*c3;
rho4=832;c4=2310; r4=rho4*c4;
%set dimensions
x1=1.5; %lead/coating boundary
x2=1.501; %coating/component boundary
%Calculate reflection/transmission coefficients at boundaries p 6-11 3451
R1=(r2-r1)/(r2+r1);
RI1=abs(R1)^2;
R2=(r3-r2)/(r3+r2);
RI2=abs(R2)^2;
R4=(r4-r3)/(r4+r3);
RI4=abs(R4)^2;
TI1=1-RI1;
TI2=1-RI2;
TI4=1-RI4;
%Print Results
fprintf('Reflection intensity at lead-coating boundary %g\n',RI1);
fprintf('Reflection intensity at coating-component boundary %g\n',RI2);
fprintf('Transmission intensity at lead-coating boundary %g\n',TI1);
fprintf('Transmission intensity at coating-component boundary %g\n',TI2);
fprintf('Reflection intensity at sodium-steel boundary %g\n',RI4);
fprintf('Transmission intensity at sodium-steel boundary %g\n',TI4);
```

```
Reflection intensity at lead-coating boundary 0.0591231

Reflection intensity at coating-component boundary 0.00434761

Transmission intensity at lead-coating boundary 0.940877

Transmission intensity at coating-component boundary 0.995652

Reflection intensity at sodium-steel boundary 0.801794

Transmission intensity at sodium-steel boundary 0.198206
```

Published with MATLAB® R2016a

APPENDIX E. ECT PENETRATION DEPTH MATLAB CODE

```
%Determine Eddy Current Penetration Depth
clear
clc
f=100:100:25000000; %frequency range for ECT
sig=1.35e6; %conductivity of material
mu=1.28e-6; %magnetic permeability
d=1./sqrt(3.14159.*sig.*mu.*(f));
semilogx(f,d*1000)
grid on
title('ECT Penetration Depth in AISI 316(L) SS')
ylabel('Maximum Penetration Depth [mm]')
xlabel('Frequency [Hz]- log scale')
```

Published with MATLAB® R2016a

THIS PAGE INTENTIONALLY LEFT BLANK

APPENDIX F. STEEL ATTENUATION MATLAB CODE

```
%Attenuation of sound in Steel up to 10 cm thick
clear
clc
x=0:.001:.2;
A2=10.^(-x.*(.1)); %100kHz
A3=10.^(-x.*(.5)); %500kHz
A4=10.^(-x.*(1)); %1MHz
A5=10.^(-x.*(3)); %3MHz
A6=10.^(-x.*(5)); %5MHz
A7=10.^(-x.*(10)); %10MHz
plot(x*100,A2)
hold all
plot(x*100,A3)
plot(x*100,A4)
plot(x*100,A5)
plot(x*100,A6)
plot(x*100,A7)
grid on
title('Attenuation of sound in steel up to 10 cm thick')
xlabel('Distance from source [cm]')
ylabel('Relative Intensity')
legend('100kHz','500kHz','1MHz','3MHz','5MHz','10MHz')
```

Published with MATLAB® R2016a

THIS PAGE INTENTIONALLY LEFT BLANK

APPENDIX G. RELATIVE INTENSITY ACCOUNTING FOR ATTENUATION AND REFLECTION-TRANSMISSION

```
%Attenuation of sound in lead at 753K vs Sodium
%For a distance of 4.3m (RV-top of Core and return)
%5.9% reflection lead-sodium, 80.2% for Sodium
%Based on attenuation for 1MHz
clear
clc
x=0:.01:9.5;
  A1=.059*10.^(-x.*(.0838)); %lead
  A2=.80*10.^(-x.*(.2600)); %Sodium
plot(x,A1)
hold all
plot(x,A2)
grid on
title('Relative Intensity across a reactor (Lead vs. Sodium) accounting for
reflection with 316(L) SS')
xlabel('Distance signal travels [m]')
ylabel('Relative Intensity')
legend('Lead','Sodium')
```

Published with MATLAB® R2016a

THIS PAGE INTENTIONALLY LEFT BLANK

APPENDIX H. POSSIBLE APPLICATIONS OF LFRS

A. MICROGRID APPLICATIONS

LFRs have many possible future applications because of their scalability and reliability. The Department of Energy proposed the integration of different energy sources for use in a microgrid (Bower et al., 2014). "A microgrid is a discrete energy system consisting of distributed energy sources (including demand management, storage, and generation) and loads capable of operating in parallel with, or independently from, the main power grid" (General Micro Grids, 2017). Currently there are 124 microgrids operational in the United States (Boyce, 2015) providing over 1,100 MW of electricity. Although most of these are traditional power plants or renewable energy sources, LFRs provide a promising alternative to meet both DOE and DOD objectives.

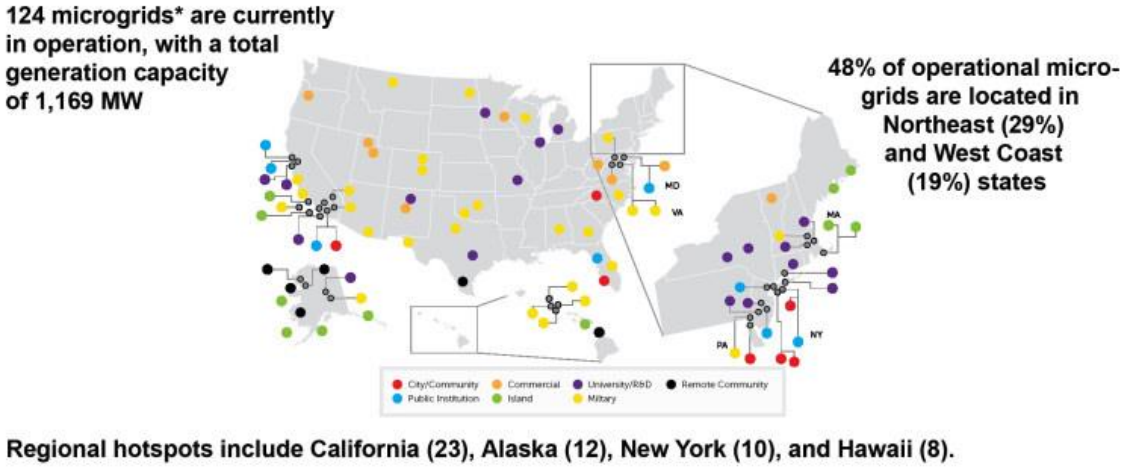

Figure 18. Operational Microgrids in the US. Source: Boyce (2015).

Microgrids work in a unique way to supplement the current power distribution system, without altering current infrastructure. In a traditional power grid, the power goes straight from the power generation company to the consumer. In the event of a disconnection or power failure, the system fails. In a microgrid, there are three tiers of protection (Bower et al., 2014). The largest power source remains a traditional power

generator. The secondary source is a localized energy source, which can operate in parallel with a larger generator or as an “island,” separately from the main power grid in the event of a failure. The third power source is a small, local renewable source that offsets power distribution requirements. In combination, these power sources provide large traditional power with a reliable secondary backup and cheap renewable supplemental power source.

Microgrids can provide primary or load following power from a traditional power plant. In a primary power system, microgrid power can come from a traditional power plants at a smaller localized level. These base load power plants run continuously. In load following microgrids, the power source adjusts its output as demand fluctuates (Bower et al., 2014) to meet power requirements in the event of a primary power source failure. This can be done by a traditional power plant with flexible power output, or by storing energy in batteries or other mechanisms to release at peak times. In both situations, a microgrid gives reliability in the event of a failure, minimizes energy losses through transmission, and places control at the local level.

Using LFRs as tier of protection in a primary power role is an efficient way to secure our current energy grid. LFRs (or reactors in general) are traditionally base power sources producing full power when operating continuously. This makes them inefficient in a load following, secondary tier protection role without massive amounts of battery or other energy storage.

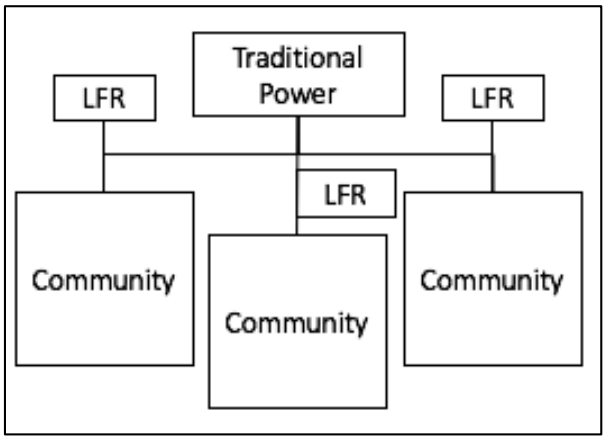

Figure 19. LFR Integration in a Microgrid Concept Sketch.

The ability to scale LFRs to meet individual community requirements means a traditional load following power plant (e.g., fossil fuel burning) can be connected to multiple communities as secondary power source, each with its own dedicated LFR. Because the fossil fuel burning plant moves into a secondary role, greenhouse gas emissions are decreased while maintaining the current energy structure as a backup. In the event of one LFR or traditional power failing, the other systems can work to supplement each other and maintain power. In the event one power source becomes corrupted, the others can island themselves and protect the integrity of power supply to the individual communities. This transition makes no changes to the current energy structure, but adds a clean power source closer to the consumer, losing less power in transition and securing our energy structure.

Discussing initial choices for a microgrid power source, one might look at small renewable energy sources or load following reactors that can modulate power. Traditional load following power plants are either environmentally unfriendly (coal, gas), or not available everywhere (hydro). Although renewables may be a good addition to a microgrid infrastructure, they are not reliable enough – due to the intermittent nature - to be a primary power source and, in the case of solar or wind power, depend heavily on weather conditions. A base load nuclear reactor provides grid stability and longevity, and can be considered a green energy source. Additionally, LFRs can be hardened against natural disasters and external threats, and have internal radiation protection because of

the material properties of lead. They also allow scaling because of their low-pressure requirements and high thermal efficiency. For these reasons, LFRs should have a future place in the U.S. energy grid.

B. MILITARY APPLICATIONS—MICROGRIDS ANCHORED BY SMALL LFRS

The military has fixed bases from coast to coast and all around the world. These bases scale from the small patrol base of an infantry company, to large installations such as Fort Riley Kansas, home of the 1st Infantry Division. The diversity of installation sizes presents a unique challenge in terms of power demand requirements. With those requirements in mind, LFRs can meet military dependability and high power needs with scalability to meet tailored energy demands, deployability to power overseas installations, and the ability to provide a highly resilient autonomous microgrid power source to provide assured power in the event of natural disaster or terrorist attack.

Our military's deployed forces rely primarily on above ground diesel power generators to run their equipment. According to Army planning doctrine, the average person on a base requires .32-.36 kWh per person per day (Department of the Army, 2008). This figure was shown to be inadequate for our large Forward Operating Bases in Afghanistan. According to a "The Mechanical Engineer" white paper (Garvin and Codling, 2012), our power demand at Camp Leatherneck, Afghanistan was 5 MWh with a population of 10,000 Soldiers. This increases our figure to .5 kWh per person per day (Garvin and Codling, 2012). If you apply these statistics to our largest base in Afghanistan, Bagram Airfield, with a population of around 40,000 Soldiers, the power demand increases to between 12.8 MWh on the low planning end, to 20 MWh when compared to Camp Leatherneck. With our largest generator, the 200kW Tactical Quiet Generator, using 13.9 gal/hour (Padden, 2009), it translates to Bagram using 64–100 generators and consuming 21,000-33,000 gallons of fuel daily just in generators. This is simply not sustainable logistically or with environmental considerations in mind. The amount of fuel needed to transport the fuel alone is astronomical to sustain our larger operating bases. Our FOBs need a better solution for their power demands.

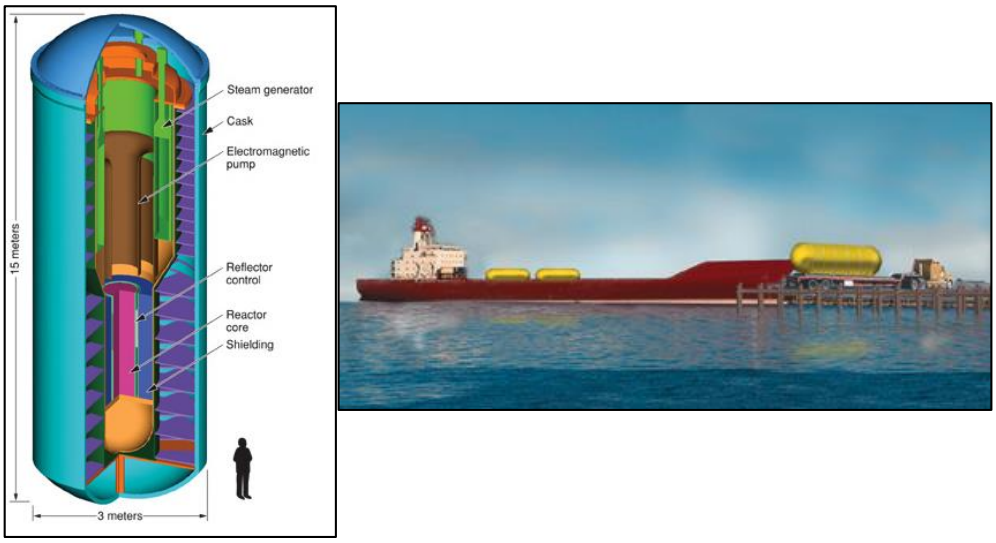

Figure 20. SSTAR Concept Design and Size Comparison. Source: Smith (2004).

A small scale LFR could be ideal for deployable operational power in our larger bases. The characteristics of lead give engineers the ability to design small scale (10-100 MWe) deployable reactors as shown in the SSTAR (Smith and Cinotti, 2016). This large power range replaces 50 Tactical Quiet Generators on the conservative side, with the ability to scale up to 500 generators, powering bases greater than 20,000 personnel with ease. Additionally, the fuel life cycle period is estimated between 15–30 years. The compactness of such a system allows the consideration of underground emplacement as a means to providing protection against kinetic or EMP attack. Overall, LFRs have the design ability for the military to consider it a viable and resilient deployable power generation option.

Another key discussion for the military is the fixed installation microgrid, and its ability to provide highly resilient and reliable energy while minimizing carbon emissions. Where the public sector has advantages in grid stability and power efficiency in the transition to a microgrid, the military looks for backup power sources for critical infrastructure to minimize down time. In the event of a natural disaster, attack, or some unforeseen event, a microgrid can act to keep hospitals and headquarters buildings running. This facilitates command, control, and medical functions in the event of external grid power failure. Additionally, the DOD has enormous power demand needs in the

United States and abroad, making it an ideal way for the government to reduce carbon emissions. In 2012, the Department of Defense made a commitment to install three gigawatts of renewable energy on its facilities by 2025 (Holland et al., 2013), to enhance grid stability and reduce its carbon footprint. This supports the overall goals of grid stability, critical infrastructure protection, and reduction of carbon emissions.

In 2011, the military began a joint project called the Smart Power Infrastructure Demonstration for Energy Reliability and Security (SPIDERS) to investigate power generation options available and demonstrate the ability for bases to operate as part of an integrated microgrid. Their goals included critical infrastructure defense from power loss for prolonged periods, integrating renewable energy sources, and reducing the overall carbon footprint of energy sources (NAVFEC, 2015), aligning with the Department of Defense goals. Over the course of four years and testing on three bases, the Army successfully integrated solar power arrays, battery storage, and backup generators to supplement power losses on a small scale (1-3MW). At the conclusion of their study, the assessment team found they relied on generators due to intermittent solar conditions and limited battery storage. The base also had inadequate fuel storage for their generators in the event of a long-term power outage. Without adequate sunlight, the study found their test base could last about five days on backup generators before fuel became an issue. SPIDERS was a step in the right direction, but not reliable enough to scale with battery and fuel storage requirements.

LFRs can meet the DOD goal of reducing carbon emissions, while providing autonomous power for continuous operations in the event of an external (grid) power failure. Although the intent of SPIDERS was to integrate solar power to reduce costs and offset power outages, it proved the military still relies heavily on stored diesel fuel and generators in contingency operations. Using generators runs counter to the goal of reducing carbon emissions. On the other side, LFRs can scale for individual power requirements and are reliable in the event of natural disasters. They are a “green” technology with the only significant output emission as water vapor. LFRs scaled above the base power requirements allow for expansion, and feed power back into the civilian grid, supporting grid stability during peak times, and providing adequate power during an

islanded situation when the civilian grid fails. This meets the DOD goals for stability, reduction of CO_2 emissions, and powering of critical infrastructure in power failures.

Overall, reactors cooled by lead or lead bismuth have many potential applications for future military use. Modular, deployable, scaled reactor systems can enhance large deployment operations or critical infrastructure power requirements. The properties of lead/LBE as a moderator give the ability to make inherently safe dedicated reactor systems for military needs.

THIS PAGE INTENTIONALLY LEFT BLANK

LIST OF REFERENCES

Accuratus. 2013. "Aluminum Oxide, Al_2O_3 Ceramic Properties." http://accuratus.com/alumox.html.

AZO Materials. 2017. "Stainless Steel - Grade 316 (UNS S31600)." Accessed 17 March. http://www.azom.com/properties.aspx?ArticleID=863.

Bower, Ward Isaac, Dan T. Ton, Ross Guttromson, Steven F. Glover, Jason Edwin Stamp, Dhruv Bhatnagar, and Jim Reilly. 2014. *The Advanced Microgrid. Integration and Interoperability.* No. SAND2014--1535. Albuquerque, NM (United States): Sandia National Laboratories (SNL-NM).

Boyce, Dan. 2015. "Military Marches Forward with Microgrids." Inside Energy. Last modified July 9. http://insideenergy.org/2015/07/09/military-marches-forward-with-microgrids/.

BWXT. 2017. "PWR Steam Generator Tube Inspections." Accessed 17 March. http://www.bwxt.com/nuclear-energy/utility-solutions/services/sghx-services/pwr-steam-generator-tube-inspection

Department of the Army. 2008. General Engineering 3–34.400 (FM 5–104). Washington, DC: Headquarters, Department of the Army.

Department of Energy. 1993. *DOE Fundamentals Handbook: Nuclear Physics and Reactor Theory* (DOE-HDBK-1019/1-93). Springfield, VA: National Technical Information Services.

García-Martín Javier, Jaime Gómez-Gil, and Ernesto Vázquez-Sánchez. 2011. "Non-Destructive Techniques Based on Eddy Current Testing." *Sensors* 11(3):2525-2565. doi:10.3390/s110302525.

Garvin, Chris, and Jim Codling. 2012. "Grid Connection of Contingency Base Camps: Making it Happen." Power Engineers. Last Accessed 23 June 2017. https://www.powereng.com/white-papers/grid-connection-of-contingency-base-camps-making-it-happen/.

The Generation IV International Forum Lead-cooled Fast Reactor Provisional System Steering Committee (GIF LFR pSSC). 2015. *Safety Design Criteria for Generation IV Lead-Cooled Fast Reactor System DRAFT*. Boulogne-Billancourt, France: OECD.

General Micro Grids. 2017. "Microgrids: The Self Healing Solution." Accessed 17 March. https://www.generalmicrogrids.com/about-microgrids.

Holland, Andrew, Nick Cunningham, Kaitlyn Huppmann, and William Joyce. 2013. *Powering Military Bases: DOD's Installation Energy Efforts Fact Sheet*. Washington, DC: American Security Project.

Illinois Emergency Management Agency (IEMA). 2016. *Environmental Monitoring Program for Nuclear Power Stations Report for Calendar Year 2015*. Springfield, Illinois: IEMA.

Induceramic. 2017. "Ceramic Honeycomb-Molten Metal Filtration." Accessed 17 March. http://www.induceramic.com/industrial-ceramic-product/ceramic-honeycomb-molten-metal-filtration.

Jethra, Ravi. 2013. "Improving Temperature Measurement in Power Plants." *Power Engineering*. Last modified March 1. http://www.power-eng.com/articles/print/volume-117/issue-3/departments1/what-works/improving-temperature-measurement-in-power-plants.html.

Kinsler, Lawrence E., Austin R. Frey, Alan B. Coppens, James V. Sanders. 2000. *Fundamentals of Acoustics*, *Fourth Edition*. New York, NY: John Wiley & Sons, Inc.

Koerner, R. M., W. M. McCabe, and A. E. Lord. 1981. *Acoustic Emissions in Geotechnical Engineering Practice*. Philadelphia, PA: ASTM International.

Naval Facilities Engineering Command (NAVFEC). 2015. "Smart Power Infrastructure Demonstration for Energy Reliability and Security (SPIDERS) Technology Transition Final Public Report." Report GFI072414122826DEN. Washington, DC: U.S. DOD.

OECD Nuclear Energy Agency (OECD/NEA). 2014. *Technology Roadmap Update for Generation IV Nuclear Energy Systems.* Boulogne-Billancourt, France: OECD.

Pacific Northwest National Lab (PNNL). 2009. *Under-Sodium Viewing: A Review of Ultrasonic Imaging Technology for Liquid Metal Fast Reactors*. PNNL-18292. Springfield, VA: National Technical Information Services.

Padden, Michael. 2009. "Tactical Electrical Power, Now and for the Future." Presented at *Joint Service Power Expo*. New Orleans, LA: Department of Defense, Project Manager Mobile Electric Power (PM MEP).

Pajnić, Mladen, Krunoslav Markulin, Alojzije Matokovic, and Hrvoje Franjić. 2010. "Advanced Approach of Reactor Pressure Vessel In-Service Inspection," 10th European Conference on Non-Destructive Testing June 7–11, 2010, Moscow Russia: RSNTTD.

Sobolev, Vitaly. 2010. “Database of Thermophysical Properties of Liquid Metal Coolants for GEN-IV.” Scientific Report of the Belgian Nuclear Research Center. Boeretang, Belgium: SCK-CEN.

Smith, Craig F. 2004. “Nuclear Energy to Go: A Self-contained, Portable Reactor.” *Science and Technology.* https://str.llnl.gov/str/JulAug04/Smith.html.

Smith, Craig F., William G. Halsey, Neil W. Brown, James J. Sienicki, Anton Moisseytsev, and David C. Wade. 2008. “SSTAR: The U.S. Lead-cooled Fast Reactor (LFR).” *Journal of Nuclear Materials.* doi: 376.3: 255–259.

Smith, Craig F., and Luciano Cinotti. 2016. “Lead-cooled Fast Reactor,” In *Handbook of Generation IV Nuclear Reactors, 1st Edition*, edited by Igor Pioro. Sawston, Cambridge: Woodhead Publishing.

Tarantino, Mariano, Luciano Cinotti, and David Rozzia. 2012. “Lead-Cooled Fast Reactor (LFR) Development Gaps.” In *Proceedings of the 2012 Technical Meeting to Identify Innovative Fast Neutron Systems Development Gaps, International Atomic Energy Agency*. Vienna, Austria: IAEA.

United States Nuclear Regulatory Commission (US NRC). 2015. “Pressurized Water Reactors.”. Last modified January 15. https://www.nrc.gov/reactors/pwrs.html.

United States Nuclear Regulatory Commission (US NRC). 2017. “Guidance for Developing Principal Design Criteria for Non-Light Water Reactors.” Proposed Amendment to *Appendix A, Part 50, Title 10 of the Code of Federal Regulations.* Draft Regulatory Guide DG-1330. Rockville, MD: U.S. NRC.

Westinghouse Electric Company, LLC. 2016. “Attachment 4: Demonstration Lead-cooled Fast Reactor Details: Westinghouse Lead-cooled Fast Reactor.” RT-TR-15-30 Revision 1. Monroeville, PA: Westinghouse Electric Company, LLC.

Wilson, Oscar B. 1988. *Introduction to Theory and Design of Sonar Transducers, Expanded edition*. Los Altos Hills, CA: Peninsula Publishing.

THIS PAGE INTENTIONALLY LEFT BLANK

INITIAL DISTRIBUTION LIST

1. Defense Technical Information Center
   Ft. Belvoir, Virginia

2. Dudley Knox Library
   Naval Postgraduate School
   Monterey, California